SECURITY CLASSIFICATION OF THIS PAGE

AD-A235 168

REPORT DOCUMENTATION PAGE

Form Approved OMB No. 0704-0188

1a. REPORT SECURITY CLASSIFICATION

1b. RESTRICTIVE MARKINGS

2a. SECURITY CLASSIFICATION AUTHORITY

3. DISTRIBUTION/AVAILABILITY OF REPORT
APPROVED FOR PUBLIC RELEASE:
distribution is unlimited

2b. DECLASSIFICATION/DOWNGRADING SCHEDULE

4. PERFORMING ORGANIZATION REPORT NUMBER(S)

5. MONITORING ORGANIZATION REPORT NUMBER(S)
AFOSR-TR- 91 [illegible]

6a. NAME OF PERFORMING ORGANIZATION
Georgia Institute of Technology

6b. OFFICE SYMBOL (If applicable)

7a. NAME OF MONITORING ORGANIZATION
Air Force Office of Scientific Research

6c. ADDRESS (City, State, and ZIP Code)
School of Materials Engineering
Atlanta, Georgia 30332

7b. ADDRESS (City, State, and ZIP Code)
Electronic and Materials Sciences
Building 410
Bolling AFB D.C. 20332

8a. NAME OF FUNDING/SPONSORING ORGANIZATION
AFOSR

8b. OFFICE SYMBOL (If applicable)

9 PROCUREMENT INSTRUMENT IDENTIFICATION NUMBER
AFOSR-87-0162

8c. ADDRESS (City, State, and ZIP Code)
Electronic and Materials Sciences
Building 410
Bolling AFB D.C. 20332

10 SOURCE OF FUNDING NUMBERS

PROGRAM ELEMENT NO.	PROJECT NO.	TASK NO	WORK UNIT ACCESSION NO.
61102	2306	A1	

11. TITLE (Include Security Classification)
Cyclic Deformation, Damage, and Effects of Environment in the Ni_3Al Ordered Alloy at Elevated Temperature

12. PERSONAL AUTHOR(S)
Stephen D. Antolovich and Graham Webb

13a. TYPE OF REPORT	13b TIME COVERED	14 DATE OF REPORT (Year, Month, Day)	15. PAGE COUNT
Final Technical Report	FROM 12-1-87 TO 12-1-90	March 29, 1991	103

16. SUPPLEMENTARY NOTATION

17. COSATI CODES		
FIELD	GROUP	SUB-GROUP

18 SUBJECT TERMS (Continue on reverse if necessary and identify by block number)
Dynamic Embrittlement
Cr Effect
Grain boundary cracking
Cr-B particles
Fatigue Crack Propagation
Thermal reversibility

19. ABSTRACT (Continue on reverse if necessary and identify by block number)

The objective of this study is an experimental determination of the effect of composition, temperature, and environment on the fatigue crack propagation resistance of Ni_3Al polycrystalline alloys. The experimental portion of the report describes these results in which the important metallurgical variables were identified. In addition, an analytical model for yielding based upon the concept of cross-slip equilibria is introduced. Th model utilizes a thermodynamic framework which is consistent with all presently observed characteristics of yielding in Ni_3Al, including strain rate independence and thermal reversibility. Complete thermal reversibility was experimentally observed in polycrystalline Ni_3Al which lends futher credence to the model.

Two alloy compositions were evaluated with the same equivalent stoichiometry and processing history. Both alloys were single phase, substoichiometric B-doped compositions, one binary Ni-Al, one ternary Ni-Al-Cr. Following initial processing, the

20 DISTRIBUTION/AVAILABILITY OF ABSTRACT
☐ UNCLASSIFIED/UNLIMITED ☐ SAME AS RPT ☐ DTIC USERS

21 ABSTRACT SECURITY CLASSIFICATION
UNCLASSIFIED

22a. NAME OF RESPONSIBLE INDIVIDUAL
~~Stephen D. Antolovich~~ Klaus Klier

22b. TELEPHONE (Include Area Code)
~~404-894-3012~~ 202-767-4933

22c. OFFICE SYMBOL
NE

DD Form 1473, JUN 86 Previous editions are obsolete

SECURITY CLASSIFICATION OF THIS PAGE
UNCLASSIFIED

DTIC COPY

91 5 01 009

DTIC ELECTE MAY 02 1991 S E

Block 19 cont.

mean linear intercept grain size of the ternary alloy was 3 times smaller than that of the binary alloy. An additional heat treatment was used to grow identical grain sizes in the binary and ternary alloys. These alloys were then used to evaluate the Cr effect on the elevated temperature deformation properties. The materials were subjected to tensile, low cycle fatigue and fatigue crack propagation testing at ambient and elevated temperature in both air and vacuum environments. The results from static and cyclic testing indicated that the grain boundary cohesive strength of the Ni-Al-Cr ternary alloys was lower than that of the Ni-Al alloys at ambient temperatures. At elevated temperatures, stress-assited oxygen diffusion along grain boundaries significantly reduces the grain boundary strength of the Ni-Al alloys and results in degredation of the mechanical properties. This effect is far less pronounced in the ternary alloy as the Cr additions were found to reduce the degradation of grain boundary strength at elevated temperatures. This occurs by reduction of the grain boundary diffusivity of oxygen in the Cr_2O_3 oxide which is extremely dense and resistant to spalling.

CYCLIC DEFORMATION, DAMAGE, AND EFFECTS OF ENVIRONMENT IN THE Ni_3Al ORDERED ALLOY AT ELEVATED TEMPERATURE

PREPARED BY:

Stephen D. Antolovich

Professor and Director
School of Materials Engineering
Georgia Institute of Technology
Atlanta, Georgia 30332

Graham Webb
Graduate Research Assistant
School of Materials Engineering
Georgia Institute of Technology
Atlanta, Georgia 30332

Technical Report

Final Report for period 12-1-87 through 12-1-90
Contract No. AFOSR-87-0132

Air Force Office of Scientific Research
Electronic and Materials Sciences
Building 410
Bolling AFB, D.C. 20332

Program Manager: Dr. A.H. Rosenstein

ABSTRACT

The objective of this study is an experimental determination of the effect of composition, temperature and environment on the fatigue crack propagation resistance of Ni_3Al polycrystalline alloys. The experimental portion of the report describes these results in which the important metallurgical variables were identified. In addition, an analytical model for yielding based upon the concept of cross-slip equilibria is introduced. The model utilizes a thermodynamic framework which is consistent with all presently observed characteristics of yielding in Ni_3Al, including strain rate independence and thermal reversibility. Complete thermal reversibility was experimentally observed in polycrystalline Ni_3Al which lends further credence to the model.

Two alloy compositions were evaluated with the same equivalent stoichiometry and processing history. Both alloys were single phase, substoichiometric B doped compositions, one binary Ni-Al, one ternary Ni-Al-Cr. Following initial processing, the mean linear intercept grain size of the ternary alloy was 3 times smaller than that of the binary alloy. An additional heat treatment was used to grow identical grain sizes in the binary and ternary alloys. These alloys were then used to evaluate the Cr effect on the elevated temperature deformation properties. The materials were subjected to tensile, low cycle fatigue and fatigue crack propagation testing at ambient and elevated temperature, in both air and vacuum environments. The results from static and cyclic testing indicated that the grain boundary cohesive strength of the Ni-Al-Cr ternary alloys was lower than that of the Ni-Al alloys at ambient temperatures. At elevated temperatures, stress-assisted oxygen diffusion

along grain boundaries significantly reduces the grain boundary strength of the Ni-Al alloys and results in degredation of mechanical properties. This effect is far less pronounced in the ternary alloy as the Cr additions were found to reduce the degradation of grain boundary strength at elevated temperature. This occurs by reduction of the grain boundary diffusivity of oxygen in the Cr_2O_3 oxide which is extremely dense and resistant to spalling.

TABLE OF CONTENTS

LIST OF TABLES

1. INTRODUCTION

Currently high temperature, high stress applications in the aerospace industry are almost entirely dominated by the use of superalloys. It is widely recognized that the development of conventional nickel superalloys has reached a point of diminishing returns. Further increases in use temperature (resulting in increased efficiency) will be achieved through the development of new higher temperature material systems. Towards this end, material systems that possess long range order (LRO) have been selected. The term LRO implies that the atoms in these alloys occupy specific sublattice sites and form superlattice structures. In general, the strength of these alloys does not degrade rapidly with increasing temperature, and in some cases the flow stress actually increases. Long range order produces stronger binding and closer packing between atoms which restricts atomic mobility leading to slower diffusion and perhaps better creep resistance. Ordered intermetallics such as aluminides and silicides are generally resistant to both oxidation and corrosion due to the ability to form dense, adherent, oxide surface films.

Although possessing several desirable characteristics, ordered intermetallic alloys are, in general, brittle. It is this characteristic that has limited their application. The brittleness is attributable to low crystallographic symmetry and/or grain boundary weakness. Low crystallographic symmetry limits the number of permissible slip systems which results in brittle intergranular fracture rather than plastic flow. Grain boundary weakness occurs from low grain boundary coherent strength, due to differences in electronegativity and atom size, limited mobility of grain boundary dislocations, or a combination of both of these mechanisms.

Recently, increases in intermetallic ductility have been demonstrated through control of metallurgical variables. One well known example is the ability of small B additions to ductilize ordered Ni_3Al [1]. Such demonstrations have increased interest for the use of such materials for high temperature applications.

In the present study, the Ni_3Al ordered material system is examined. This material possesses the $L1_2$ (FCC derivative) structure with Ni atoms on face centered lattice sites and Al atoms on corners (figure 1.1). Binary Ni_3Al is ductile as a single crystal, but brittle as a polycrystal [2]. Examination of polycrystal fracture surfaces reveal intergranular fracture. These observations imply that grain boundary weakness controls the ductility of this material system. As alluded to previously, small additions of B (0.028 wt%) in Ni rich (hypostoichiometric) alloys have resulted in large ambient temperature elongations and transgranular fracture [1]. At elevated temperatures in vacuum environments, the compositional modifications continue to ductilize Ni_3Al up to its melting point [3]. However, in the presence of oxygen, intergranular fracture and low ductility again result [4]. These observations imply that at elevated temperature environmental attack of the grain boundaries produces low ductility and intergranular fracture. It has since been discovered that the elevated temperature environmental sensitivity can be reduced by Cr additions [5].

Based upon these preliminary results, it appears that Ni_3Al alloys show promise for consideration as high temperature structural materials. At this point, further evaluation of the mechanical properties of these materials (specifically creep, oxidation and fatigue) must be evaluated before implementation in structural applications. At present, understanding of the effect of cyclic loading at ambient and elevated temperatures is limited. In addition,

the effects of environment on cyclic deformation are not well understood. Such information is essential if the goal of utilizing intermetallics in structural components is to be met.

Towards this end, the current research program was conducted. The program combined mechanical testing, microscopy, and analytical studies to identify mechanisms which determine the fatigue response of polycrystalline Ni_3Al alloys. The experimental program variables were composition, temperature, strain rate, and environment. Such testing enabled evaluation of the important metallurgical variables which control cyclic deformation. In addition, new advances were made in modeling the deformation response of Ni_3Al alloys at elevated temperatures. This information will be indispensable in developing LRO alloys to their maximum usefulness, as well as providing further insight into the deformation response of Ni-base superalloys which are strengthened by Ni_3Al precipitates.

2. BACKGROUND

2.1 Dislocations in Ni_3Al

There are several important differences between the deformation characteristics of ordered and disordered materials that can be directly related to the presence of long range atomic order. In the specific case of ordered $L1_2$ materials, the superlattice structure constrains the flow of the dislocations, by controlling core characteristics [6]. In Ni_3Al and like $L1_2$ alloys, several different combinations of dislocations and faults have been proposed [7]. The nature of these dissociation are dependent upon both alloy composition and temperature.

Computer simulations of the core configuration of dislocations in $L1_2$ ordered materials [6,8,9] have determined that non-planar core configurations exist in $L1_2$ ordered materials. The most important implication of this results is that components of the stress tensor which do not exert a resolved shear stress on the dislocation can have a large effect on the flow properties by altering the core dissociation [10-12]. Such an effect has been shown to be very important in determining the flow properties of Ni_3Al alloys.

A given dislocation in a $L1_2$ superlattice can dissociate in a number of ways, depending upon which faults are stable and how long the Burgers vectors are. Here only faults on {111} and {010} planes are considered as these are the important slip planes in $L1_2$ materials [11]. On {111} (octahedral) planes many different fault dissociations and associated dislocation configurations can occur (figure 2.1) [7], while on {010} (cube) planes, only one type of dissociation occurs [13].

It is well known that unit dislocations in disordered lattices are only partial

dislocations in the superlattice of ordered materials. These partials must either combine to form larger dislocations with Burgers vector equal to a primitive lattice translation, or occur in pairs separated by a strip of antiphase boundary (APB). The latter type of dislocation is known as a "superdislocation". APB coupled dislocations can occur on either octahedral or cube planes and are demonstrated in figure 2.1(a). It was further noted that each of the paired dislocations joined by APB on {111} (termed superpartials) can additionally dissociate into two Shockley partials of Burgers vector a/6<121> (figure 2.1(b)) connected by a stacking fault. As the stacking fault is super-imposed onto the existing antiphase boundary, the resulting combined fault is called a complex stacking fault (CSF). A third fault that can occur on {111} in $L1_2$ structures results from the dissociation of the unit dislocation by the shear vector a/3<112> (figure 2.1(c)) which produces a fault known as the superlattice intrinsic stacking fault (SISF) bound by two partial dislocations. All three of these faults can occur simultaneously according to the scenario demonstrated in figure 2.1(d). A final possibility occurs when two SISF bound partial dislocation pairs overlap on adjacent {111} planes (figure 2.1(e)) resulting in a fault known as a superlattice extrinsic stacking fault (SESF). Direct observations of dislocations using both TEM and HREM techniques have revealed dislocations dissociated in Ni_3Al by all of the above scenarios [10,12,14-22].

2.2 Deformation in Single Crystal Ni_3Al

In most crystalline, dislocation flow dictates material plasticity, which in turn controls fatigue properties. Due to this, a through understanding of dislocation mechanisms is

essential for understanding fatigue processes. The strength of Ni_3Al has been observed to possess three different deformation regimes as temperature increases (figure 2.2), where each regime is associated with a change in the sign of $d\tau/DT$ [10,11,20,23-25]. The initial regime is associated with a decreasing flow stress with temperature. The second regime is characterized by a positive increase in shear stress with temperature. The third and final regime is once again characterized by negative $d\tau/DT$ which is separated from regime II by a peak value. The temperatures where the various regimes end and begin are observed to depend on composition and crystallographic orientation. The principal operating slip system in regime I and II is $\{111\}<110>$ (primary octahedral slip). The principal operating slip system in regime III is $\{010\}<110>$ (primary cube slip).

In regime I, the observed variation in shear stress with temperature is considered to be related to the variation in shear modulus with temperature [10,11,20,23-25]. When tested at very low temperatures, the dislocation substructures are observed in the form of tangled edge and mixed dipoles [10,20,21,23] and SISF bound dislocation loops [10,20,21]. In this regime, deformation is considered to occur similar to that observed in FCC materials.

Regime II, where the flow stress increases with temperature (*i.e.* anomolous flow) covers the largest range of temperatures and has received the greatest amount of attention. In this temperature regime the material possesses several unusual deformation characteristics including:

1. Schmid's law is not obeyed [10].
2. Orientation dependent tension-compression asymmetry [11].
3. Strain rate independence [14].
4. Thermal reversibility [2].

Observations of samples deformed in this region have noted long, straight dislocations of screw orientation [7,10,11,14-21,23]. Due to the ability of screw dislocations to cross-slip during glide, several theories have been proposed to describe the motion of screw dislocations in Regime II. These models propose that the observed anamolous behavior is related to thermally activated cross-slip from glissile to sessile planes during deformation [10-12,26,27]. These theories and others will be discussed in section IV.

Deformation in region III obeys Schmid's law and is strain rate sensitive [10,25]. Deformation in the high temperature regime is observed to occur by both edge, screw and mixed dislocations gliding on non-close packed planes {100} [10,28]. In this regime deformation can be thought of as a normal slip process on an abnormal slip plane.

2.3 Deformation of Polycrystalline Ni_3Al

Although it is known that single crystals of Ni_3Al are highly ductile, polycrystalline materials were observed to be extremely brittle, fracturing in an intergranular fashion [2]. The brittle behavior was observed to be an intrinsic material property (*i.e.* not due to impurities) related to grain boundary weakness [29]. The intrinsic brittleness was determined to be related to differences in valency, electronegativity, and atom size between nickel and aluminum atoms in Ni_3Al [30-33]. It was this fundamental brittleness which was the major obstacle to the development of Ni_3Al as a structural material.

Aoki and Izumi [1], first determined that manipulation of material variables can increase the ductility of Ni_3Al. They observed that micro-alloying Ni_3Al with B imparts substantial ductility. Liu *et al* [3] later determined that the optimum ductility is obtained

using 0.25 wt % B in hypo-stoichiometric (*i.e.* Ni rich) Ni_3Al. The ductility increase is associated with a change in fracture morphology from transgranular to intergranular.

2.3.1 Ductilization Mechanisms

Auger Electron Spectrophscopy (AES) [3,29-33] and other techniques [34-37] were used to determine the composition of grain boundaries in B ductilized alloys. These investigations revealed that B segregates to grain boundaries [3,30,33-35,37], substitutes interstitially [3,32,36,37], and that the concentration of Ni is higher within grain boundaries [3,33,34].

Although there is general agreement as to the composition of grain boundaries in Ni_3Al, there are essentially two different mechanisms to explain ductilization of Ni_3Al by boron additions and changes in alloy stoichiometry. The first mechanism, as first proposed by Liu *et al* [3] contends that the boron additions change grain boundary chemistry and increases their cohesive strength. This theory has received validation from various calculations of grain boundary cohesive strength as a function of boron content and stoichiometry [38-40], which predict strong, highly directional atomic bonding within the strongly ordered lattices of Ni_3Al. The directional bonding places compatibility requirements upon the lattice which are best satisfied in the presence of B in Ni rich Ni_3Al [39,40] for which the boundary is stronger than the bulk lattice.

A second mechanism for explaining the observed ductility is that the B disorders the boundaries. This disordering facilitates grain-boundary slip and dislocation transmission [37,41]. This effectively reduces slip band stress concentration at grain-boundary intersections. Ductility is enhanced as the stress applied to the grain boundary is lowered

[41]. Problems with this theory are due to lack of unambiguous evidence for a change from the ordered $L1_2$ structure to a disordered phase at grain boundaries.

2.3.2 Elevated Temperature Environmental Effects

Although Ni_3Al alloys exhibit good oxidation resistance, elevated temperature ductility is sensitive to environments at elevated temperatures [4,42-46]. When tested in air environments, it was determined that ductility increases initially with temperature, then degrades, reaching nil-ductility at 500-750°C (figure 2.3). The ductility drop with temperature was associated with a gradual change in fracture morphology from initially transgranular at low temperatures to totally intergranular at the ductility minimum. Liu *et al* [4,42-46] later determined that the high ductility and transgranular fracture characteristic of ambient temperature deformation were maintained at 600°C in vacuum environments, but not in air [42-46] or relatively low oxygen partial pressure [4]. A dynamic embrittlement mechanism was proposed involving:

1. Localized grain boundary stress concentration
2. Elevated temperature
3. The presence of gaseous oxygen.

By this mechanism, at elevated temperatures, oxygen is chemisorbed within grain boundary crack tips. This weakens the atomic bonding there and decreases the crack growth resistance of the material. The lack of overall ductility is caused by continuous embrittlement of fresh crack tip material which subsequently propagates the crack along the boundary. It is important to note that this mechanism does not involve oxidation, or even oxygen diffusion as the degree of embrittlement has been observed to be solely dependent upon the presence of oxygen when stress is applied at elevated temperatures [43,44].

Currently there are two known techniques for overcoming elevated temperature environmental embrittlement of Ni_3Al [5,46]. The first is to eliminate grain boundaries oriented perpendicular to the stress axis (i.e. eliminate the normal stress across the boundaries) [46]. This was demonstrated by testing Ni_3Al with columnar grain structure produced by a directional solidification technique. When tested with grain boundaries oriented parallel to the stress axis, high ductility and transgranular fracture was observed up to 700° C [46].

The second technique to create high temperature ductility is to alloy with moderate amounts of the strategic element Cr [5]. Figure 2.4 demonstrates the effect of Cr additions on the elevated temperature tensile elongation of Ni_3Fe alloys which behave similarly to Ni_3Al. Cr additions are thought to promote the formation of dense tenacious oxide at the grain boundaries which reduces exposure to gaseous oxygen and thus environmental embrittlement at elevated temperatures.

2.4 Fatigue of $L1_2$ Ordered Alloys

Currently, there is only a small body of knowledge regarding the deformation and fatigue crack growth mechanisms that occur in polycrystalline Ni_3Al. Cyclic deformation studies are primarily for single crystals of $L1_2$ alloys [47-51], with only one investigation for polycrystal behavior at elevated temperatures [21]. Several FCP investigations for polycrystalline materials [52-55] have been conducted with the results presented in the form of Paris-growth law curves for ambient and elevated temperatures.

2.4.1 Characteristics of Cyclic Deformation

Cyclic deformation experiments on various single crystal $L1_2$ alloys [47-50] have revealed that the orientation dependent tension-compression asymmetry is stable during cyclic deformation at temperatures below peak strength [47-50]. For most experiments, significant cyclic hardening was observed. The rise in cyclic stress was dependent upon temperature, crystal orientation and strain range applied [47-49]. In general, cyclic hardening continued to failure except for low cyclic strain amplitudes or for temperatures beyond peak (*i.e.* Regime III), where a saturation stress was achieved prior to failure. Cyclic softening was not observed during cyclic deformation of the single crystals.

During cyclic loading, deformation was observed to be inhomogeneously distributed within slip bands. These slip bands then initiated final fracture from the stress concentration. TEM observations of the deformed specimens revealed the presence of long straight screw dislocations [48,51], as well as dislocation debris from dislocation interactions. Bonda *et al* [51] reported the debris to be in the form screw and edge dipoles. Hsiung *et al* [48] reported a/3[111] Frank loops within slip bands presumably generated by intersection of mobile dislocations during cyclic loading. The loops were assumed to form by coalesence of defect clusters which reduced the volume decrease within slip bands. The change in volume was reported to place the slip bands in a state of residual tension which resulted in crack nucleation.

Dowling [28] investigated the cyclic response of boron-modified hypostoichiometric polycrystals with 0.5% Hf at 600° C in air and vacuum environments. During plastic strain control cycling it was observed that the cyclic strength in compression was always greater

than in tension. Cyclic hardening to saturation occurred independent of environment, although when tested in air, fracture preceded saturation in some cases. Increasing the strain rate by an order of magnitude (from 0.001/s to 0.01/s) doubled the fatigue life at a given plastic strain range. When tested in vacuum environments, the fatigue life increased by two orders of magnitude. Slip band traces were observed in samples tested to stress saturation, indicating that deformation was inhomogeneous. TEM observations revealed the presence of long straight screw dislocations. When tested in vacuum significant amounts of dislocation debris were also observed, which were not present in specimens tested in air. In air, fracture initiated at grain boundaries, with an intergranular fracture morphology. In vacuum, cracks were observed to nucleate at Hf rich islands located at grain boundaries which which then propagated in a transgranular fashion. It was concluded that fatigue in air was controlled by environmental embrittlement of the grain boundaries. The large improvement in life when tested in vacuum was attributed to the removal of gaseous oxygen and the subsequent elimination of dynamic embrittlement [4].

2.4.2 Fatigue Crack Propagation

In recent years several investigations have measured the crack growth rates of Ni_3Al at both ambient and elevated temperatures [51-54]. These investigations have revealed that fatigue crack growth rates increase with increasing temperature. This increase was consistent with a fracture morphology that continuously evolved from transgranular at ambient temperature to completely intergranular at 500-600° C [52-54]. When tested in vacuum environments, transgranular fracture was observed when tested at 600° C [54]. Crack

growth rate was found to be frequency dependent at elevated temperature, with increase growth rate for lower frequencies [53,54]. It was determined that at ambient temperatures Cr bearing alloys have a higher crack growth rate than comparable binary alloys. When tested at elevated temperatures, the crack growth rates of the Cr bearing alloys were lower than binary alloys when tested in both air and vacuum environments.

From these observations, an environmental mechanism assisted by increased temperature in the presence of the crack tip was described (identical to Liu's mechanism [4]). All investigators [52-54] accounted for changes in crack growth rates to an ever increasing amount of grain boundary embrittlement that occurred as temperature increased. As transgranular fracture is expected to absorb more plastic work then intergranular fracture, the increase in crack growth rates at elevated temperature is related to an increase in the amount of intergranular fracture. At present little is understood of the relationship between crack tip deformation and crack growth at both ambient and elevated temperatures.

3. EXPERIMENTAL VARIABLES

3.1 Program Variables

The experimental variables selected for evaluating the static and cyclic deformation characteristics of the polycrystalline alloys were; composition (Ni-Al-B and Ni-Al-Cr-B), temperature (25°, 300°, 600°C), strain rate (10^{-4}/sec and 10^{-2}/sec), and environment (air and vacuum). These variables were studied in tensile, low cycle fatigue (LCF) and fatigue crack propagation (FCP) testing. The tensile tests were designed to provide initial material property information which was utilized to select fatigue load and strain amplitudes as well as anticipate material fatigue response. The low cycle fatigue tests were designed to determine the evolution of fatigue deformation and damage. These test were not used to generate fatigue life data (Coffin-Manson data), but were intended to evaluate the deformation substructure occurring ahead of growing fatigue cracks. This information was then used to understand the fatigue crack propagation behavior.

Following mechanical testing, deformation and fracture mechanisms were evaluated by a variety of microscopy techniques, including SEM, TEM and optical metallography. SEM was used primarily to examine the fracture morphology of failed specimens. TEM microscopy was used to evaluate initial microstructures as well as to characterize the evolution of fatigue damage. Optical metallography was used to characterize the initial microstructures and also used to view replicas of the specimen surfaces.

X-ray diffraction was used to verify the existence of the L12 ordered lattice in the experimental alloys.

3.2 Material Description

In the experimental program two different alloy compositions were selected for experimental evaluation. One was a binary Ni-Al+B alloy similar to alloy IC-15 initially developed by Oak Ridge National Laboratory. The second alloy selected was a ternary alloy containing 8 at.% Cr and identical B content as the binary alloy. The stoichiometry of Ni and Al in the ternary alloy was adjusted to achieve an equivalent stoichiometry as that of the binary alloy. This was achieved following the criteria for ternary site substitution initially determined by Guard and Westbrook [56] based upon the direction of the solubility lobe in the ternary phase diagram of Ni-Al-Cr (figure 3.1). As the direction of the Cr solubility lobe is in a direction bisects the quasi-binary sections Ni_3Al-Ni_3Cr and Ni_3Al-Cr_3Al, it is presumed that Cr substitutes in equal amounts on Ni and Al sites. Using this idea the compositions of the alloys were specified. After specification, the alloys were produced from plasma sprayed powders. The powders were sieved and particle sizes between -180 and +400 mesh were placed into stainless steel cans. Consolidation was achieved by extrusion of the cans at 1100° C, then annealed at 1200° for 1 hour in argon. Once manufactured, the alloy compositions were characterized (Table I), and microstructures, substructures, and diffraction characteristics were evaluated [57].

These characterization procedures revealed two hypo-stoichiometric B modified Ni_3Al, one binary alloy and one ternary alloy containing Cr. The mean linear intercept grain size of the as-received binary alloy was determined to be 10.2μm, while the ternary alloy had a grain size of 3.5μm. In this alloy, the microstructure consisted of recrystallized (8μm) and partially recrystallized grains of smaller size (1μm). In order allow direct comparison

between the binary and ternary alloy, the grain size of a portion of the ternary alloy was increased to 10.1μm by heat treating at 1000° C for 128 hrs in Ar. The alloys were machined into specimens suitable for tensile (figure 3.2), low cycle fatigue (figure 3.3) and fatigue crack propagation (figure 3.4) testing.

4. ANALYTICAL MODEL FOR ANOMALOUS YIELDING IN Ni_3AL

4.1 Background

As mentioned in the previous chapter, in the range of temperatures where the strength is anomolous (Regime II, figure 2.2) there have been numerous attempts to provide a theoretical basis for predicting the numerous unusual characteristics of deformation in Ni_3Al alloys [11-15,26,27]. These models are, in one way or another, based upon the concept of thermally activated pinning of screw superdislocations during deformation. This approach was originally suggested by Kear and Wilsdorf [58] to explain work hardening in Cu_3Au. The mechanism is thermally activated cross slip of APB bound screw superdislocations from {111} planes to {010} planes which shared the common <110> burgers vector (figure 4.1). This work was first extended to describe anomolous yielding in $L1_2$ alloys by Takeuchi and Kuramoto [10]. In their theory, pinning of the dislocation line occurred by cross-slip from {111} to {010} in small localized regions. The pinning process was assumed to be thermally activated and was modelled in an Arrenhius framework. Additional work [6,8,11,59] extended these basic ideas to what has become well known as the Cross-Slip Pinning (CSP) model [12,59]. A separate earlier, but less well known approach, with nearly identical results was developed by Greenberg and co-workers [26-27,60-65]. In these models, a physical description of the yielding process in $L1_2$ alloys is provided whereby screw dislocations experience transformations from glissile to sessile forms by localized cross-slip from {111} to {010} slip planes. Glide of the glissile portions of the dislocation is hindered by the sessile portions which increases the stress necessary to cause

screw dislocations. The density of the sessile portions is dependent upon temperature which thus results in an increasing the flow stress with temperature.

From this basic mechanism, several forms of stress modified activation enthalpy were proposed [10-12,26,27,60-65] for characterizing cross-slip kinetics. In these models, the activation enthalpy for cross-slip is altered by the stresses which affect the cross-slip process. The models based upon cross-slip pinning have experienced considerable success in providing a theoretical basis for various understanding deformation in Ni_3Al including:

1. Increasing strength with temperature.
2. Violation of Schmid's law.
3. Orientation dependent tension-compression asymmetry.

Although extremely successful in several regards, the models are unable to describe all aspects of deformation, most notably the observed independence of the flow stress on strain rate. As all of the models mathematically assume a kinetic framework, a rate effect opposite to that of temperature is implicit.

During the course of the experimental work on the current project, the time dependency of cross-slip kinetics were evaluated [66]. It was discovered that cross-slip is a virtually instantaneous process. This suggests that deformation in Ni_3Al is more properly described in the context of thermodynamic equilibrium [67]. Following the theoretical developments, several experiments were conducted to test the validity of the model with the programs alloys which was met with remarkable success. In this section of the report, both the analytical and experimental developments will be reported

4.2 MODEL FORMULATION

In Ni_3Al alloys, the rate of cross-slip segment accumulation on the cube cross-slip plane (010) is determined by the balance of cross-slip rate in both directions. Using a simple energy diagram argument (figure 4.2), this can be expressed as:

$$dx/dt = (dx/dt)_{(111)\rightarrow(010)} - (dx/dt)_{(010)\rightarrow(111)} \quad (4.1)$$

Or, using Maxwell-Boltzmann statistics:

$$dx/dt = \nu\,(1-x)\exp(-G_{pin}/kT) - \nu\,x\exp(-G_{unpin}/kT) \quad (4.2)$$

where x = fraction of a screw dislocation that is cross-slipped on (010),
ν = attempt frequency,
G_{pin} = activation energy for cross-slip,
G_{unpin} = activation energy for reverse cross-slip,
k = Boltzmann's constant,
T = absolute temperature.

From this kinetic equation, an equilibrium cross-slipped fraction of the dislocation line can be defined as the length fraction x_{max} which corresponds to the steady-state condition:

$$dx/dt|_{x = xmax} = 0 \quad (4.3)$$

Combining equations (2) and (3):

$$x_{max} = [1 + \exp(\Delta G/kT)]^{-1} \quad (4.4)$$

where $$\Delta G = G_{pin} - G_{unpin} \quad (4.5)$$

If the activation energies G_{pin} and G_{unpin} are assumed to be independent of x, G_{unpin} can be eliminated in equation (4.2) using equation (4.4). This leads to:

$$dx/dt = \nu\,(1 - x/x_{max})\exp(-G_{pin}/kT) \quad (4.6)$$

4.2.1 Calculation of Enthalpy and Strain Rate Independence

Before continuing with the analysis G_{pin} will be evaluated and used to confirm that

cross-slip kinetics are virtually instantaneous. This will be accomplished by ignoring the entropy contribution to Gpin. This assumption is valid in that the configurational entropy will not limit cross-slip kinetics, although it can be expected to influence thermodynamic equilibrium. This can be accomplished using the physical picture illustrated in figure 4.3. to describe the dislocation segment in its highest energy state. From this the following expression is derived:

$$G_{pin} \approx H_{pin} = [Q_{con} - (\tau_{pe}b)bd] + [\Gamma_{010}b^2 - (\tau_{010}b)b2 \qquad (4.7)$$

or:

$$H_{pin} = Q - \tau_{111}V \qquad (4.8)$$

where:

H_{pin} = activation enthalpy for cross-slip,
Q_{con} = energy to constrict the Shockley partials on a length b,
τ_{pe} = constriction on edge component of Shockley partials,
d = equilibrium spacing of Shockley partials,
Γ_{010} = antiphase boundary energy on (010),
τ_{010} = resolved stress on (010),
τ_{111} = resolved stress on (111),
$Q = Q_{con} + \Gamma_{010}b^2$, and
$V = (\tau_{pe}/\tau_{111})db^2 + (\tau_{010}/\tau_{111})b^3$.

V is therefore a function of orientation, and is different in tension and compression due to τ_{pe}. The configuration presented here for the dislocation in its highest energy state is similar to that previously proposed by Paidar et al [12].

It will be shown later that the yield stress is a linear function of x, and that it implies:

$$\tau_{111} = (x/x_{max})\ \tau_{ys} \qquad (4.9)$$

where τ_{ys} is the critical resolved shear stress on (111). The activation energies are therefore not strictly independent of x. However, in equation (4.6), the correction for the x-dependence of activation energies would only change the linear function $(1 - x/x_{max})$ to a more complex function ranging from 1 (at x = 0) to 0 (at $x = x_{max}$), and is thus only a

second order correction.

The attempt frequency ν can also be estimated. For face-centered cubic structure, an evaluation would be $\nu = \nu_D/12$, where ν_D is Debye's atomic frequency. This was considered reasonably appropriate for use in $L1_2$ ordered structures.

An iterative algorithm was then used for numerical integration of (4.6), which resulted in x vs time curves such as that reproduced in figure 4.4. From these curves, an intrinsic characteristic time for cross-slip kinetics, t_o, was defined as the time needed to achieve 63% of x_{max}. For reference, this time is equal to $3x10^{-12}$ s for Q=0.1 eV, T=400° C, τ_{ys}=400 MPa and [123] tensile orientation.

A second time which is characteristic of extrinsic deformation, t_y, can be defined as the time necessary to achieve a characteristic deformation γ_{ch} (e.g. 0.2%) at a given strain rate $\dot{\gamma}$:

$$t_y = \gamma_{ch}/\dot{\gamma} \qquad (4.10)$$

$$\text{For } \dot{\gamma} = 100\%/\text{s}, \; t_y = 2x10^{-3} \text{ s.}$$

Comparing t_o and t_y and referring to figure 4.4 leads one to conclude that for strain rates that have been applied, the extrinsic characteristic time for yielding are much greater than the intrinsic characteristic time for cross-slip (i.e. $t_y > t_o$). Therefore, the fraction of the dislocation line on (010) achieves its equilibrium value x_{max} quasi-instantaneously independent of the strain rate applied.

As has been demonstrated, screw dislocation segments alternate from (111) to (010) at extremely high frequencies. The equilibrium state is the state for which segments cross-slip in both directions at the same rate. This implies that the dislocation will experience an

average friction stress from these pinning points. Due to this, screw dislocations are expected to remain straight when moving. At equilibrium, the applied force per unit length of dislocation (i.e. $\tau_{111}b$) is balanced by the drag force which arises from the presence of the pinning points:

$$\tau_{111}b = C_o\,(x/b) \tag{4.11}$$

or:

$$\tau_{111} = (C_o/b^2)\,x = \tau_o\,x \tag{4.12}$$

where C_o = drag force per cross-slipped segment,
x/b = segments per unit dislocation length,
$\tau_o = C_o/b^2$.

The resolved shear stress on (111) is therefore linearly related to x as was assumed previously. Using equation (4.11), figure 4.4 can be transformed into figure 4.5, where the yield stress is plotted vs the logarithm of time. The characteristic times corresponding to experimentally obtainable strain rates are indicated. Thus, for strain rates that have been experimentally applied, the characteristic times for yielding are much larger than t_o, such that the equilibrium density of pinning points x_{max} is achieved independently of strain rate. Here it is important to realize that C_o is simply the drag force exerted on the dislocation by a single pinning point and is thus independent of dislocation velocity. Indeed, it is proposed that the velocity dependence is related to the number of pinning points which forms on the dislocation line. Here it has been demonstrated that the equilibrium state is achieved quasi-instantaneously and as:

$$\tau_{ys} = \tau_o\,x_{max} \tag{4.13}$$

The observed strain rate independence of yielding in Ni_3Al [10,68,69], can be explained on the basis that dislocations move at a velocity consistent with the drag force

exerted by the equilibrium density of pinning points for the specific temperature/stress scenario.

4.2.2 A Thermodynamically Based Model for Yielding in Ni_3Al

Having demonstrated that the cross-slip kinetics are virtually instantaneous, it is the present contention that thermal strengthening in Ni_3Al is better described using a thermodynamic framework. Using equations (4.4) and (4.13), the following expression is easily derived:

$$\tau_{ys} = \tau_0/[1 + \exp(\Delta G/kT)] \qquad (4.14)$$

The functional form of τ_{ys} implies that τ_{ys} increases with temperature only if $\Delta G > 0$. In this case, the barrier height for pinning is larger than that for unpinning. It also implies that the unpinning process is favored over the pinning process and the majority of the dislocation line is therefore unpinned.

For larger values of ΔG, the exponential term in equation (4.14) is much greater than 1, and the equation can be simplified to:

$$\tau_{ys} = \tau_0 \exp(-\Delta G/kT) \qquad (4.15)$$

This provides the exponential temperature dependence of yield stress that has been widely used to correlate experimental data [10-12,26,27]. However, to correctly describe the temperature dependence of yielding, it is demonstrated here that the driving force (i.e. ΔG) should be considered instead of the activation energy G_{pin}.

Previous formulations have always focused on the activation barrier for pinning in order to describe yielding. This energy G_{pin} is certainly important, but to describe the kinetics of pinning. Using it implicitly implies a time-related process. Therefore, strain rate

independence of yielding can not be predicted using a kinetic framework.

When considering ΔG however, we are not interested in kinetics but also in the thermodynamics of pinning (i.e. the final or equilibrium state). Because the kinetics are extremely fast, the equilibrium state is achieved quasi-instantaneously, and therefore controls deformation. As a consequence, no time-dependence is expected. This provides a physical justification for the stain rate independence of yielding.

It may seem perplexing that the model implies a positive ΔG for the pinning process. A chemical analogy may help to understand the meaning of this positive sign. Indeed, in the case of the reaction:

$$A \rightleftharpoons B$$

the sign of the standard free energy change ΔG° decides whether the reaction is favored in direction 1 ($\Delta G^\circ < 0$), or in direction 2 ($\Delta G^\circ > 0$). However, even if the reaction is favored in direction 1 because ΔG° is negative, some B will be present at equilibrium. The reason is that the free energy of the system (ΔG_{sys}) will be minimized by transforming some A into some B. The sign and magnitude of ΔG° will determine what fraction of A will be transformed.

Similarly, the sign and magnitude of the driving force for core transformations decides what fraction of the dislocation line will be pinned. The free energy of the system will be minimized for pinning of small segments if ΔG is positive, and for pinning of most of the dislocation if ΔG is negative.

In summary, although the core transformation of the entire dislocation may not be energetically favorable (if $\Delta G > 0$), the system minimizes its free energy ΔG_{sys} by core

transformation of a fraction of the dislocation line. In this model, no particular assumption was made regarding the sign of ΔG, but a positive ΔG is found to be consistent with the observed temperature dependence of yielding.

The orientation dependence and tension-compression asymmetry of the yield stress have been well described by both Grinberg [26,27] and Paidar, Pope, and Vitek [12,59]: They considered the modification of the activation enthalpy due to stresses on (111) and (010) planes. Here, the similar modification is proposed for G_{pin} and G_{unpin}, which leads to:

$$\Delta G = G_{pin} - G_{unpin} = Q - (\tau_{(010)}V_1 + \tau_{pe(111)}V_2 + ...) \quad (4.16)$$

or

$$\Delta G = Q - \tau_{(111)}V \quad (4.17)$$

where V is a function of orientation, and is different in tension and compression.

4.3 Thermal Reversibility

The implications of the model presented here will now be discussed relative to known deformation characteristics of Ni_3Al. Using this model, the following deformation characteristics may be quantitatively predicted: increasing strength with temperature, orientation dependence, tension-compression asymmetry, and strain rate independence. Unfortunately, like the CSP model, the current model cannot account for the deformation substructures that have been observed in deformed Ni_3Al, most notably screw dislocations completely dissociated on {010} planes in the form of Kear-Wilsdorf (KW) locks (figure 4.1) [15,16,18,20,21]. In order to investigate this apparent discrepancy the concept of thermal reversibility was examined.

4.3.1 Cottrell-Stokes Experiments

The first determination of thermal reversibility in Ni_3Al was provided by Davies and Stoloff

[2] who conducted Cottrell-Stokes experiments on Ni_3Al alloys. These tests consisted of an initial straining at elevated temperature followed by cooling to some significantly lower temperature after which the specimen was further strained. The results of this experiment were then compared to the results of another test on identical material deformed to the same strain as the first specimen, but entirely at the lower temperature. Such comparisons provide an indication of the reversibility of deformation with respect to temperature, and as such are highly useful for evaluating the validity of deformation models in Ni_3Al.

At present there have been a number of such studies that have been conducted on Ni_3Al alloys [20,21,70]. The results of these experiments all indicate that deformation at elevated temperature only slightly affects subsequent low temperature strength. This indicates that deformation in Ni_3Al is "thermally reversible". The amount of irreversibility (i.e. strengthening after high temperature deformation) varied between the various investigations which is not surprising due to the differences in experimental conditions employed (i.e. crystal orientation, temperature, and strain amplitude). One of these investigators [70] attributed the irreversibility as evidence for the development of a dislocation substructure. At this point what must be determined is whether *initial* yielding in these alloys is completely reversible (as would be suggested by the current model) or significantly irreversible (as suggested by the presence of KW locks). Until now there has been no systematic evaluation of the characteristics of thermal reversibility. In the following section, the results from a series of Cottrell-Stokes experiments on polycrystalline Ni_3Al are presented. In these experiments, the effects of strain amplitude and initial test temperature on thermal reversibility are evaluated. The results of these experiments are then discussed

with regard to the newly proposed model as well as to mechanisms which describe the generation, glide and subsequent interaction of KW locks.

4.3.2 Experimental Procedure

The Cottrell-Stokes experiments were performed on the binary hypostoichiometric boron-modified binary Ni_3Al alloy with a 12μm mean linear intercept grain size. The testing was conducted on LCF specimens (figure 3.4) suitable for loading in either tension or compression. The Cottrell-Stokes tests were conducted in strain control using a SATEC CATS servohydraulic test machine. The specimens were induction heated in air between water cooled grips. The induction coil was adjusted such that a temperature distribution of $\pm$ 2 C was obtained in the gauge section of the coil. The initial elevated test temperatures selected were 400° and 600°C. These temperatures were chosen to be in the regime where strength is anomalous (i.e. Regime II). At 600°C, thermal activation is sufficient for some primary cube slip to occur which is not expected at 400°C [10,11,14]. The tests at 400°C were conducted in tension, and the tests at 600°C were conducted in compression as dynamic embrittlement of the grain boundaries limits the tensile failure strain at this temperature (ϵ_f < 1%) [4]. The low temperature portion of all Cottrell-Stokes tests was 25°C (room temperature). Following the elevated temperature testing, the specimens were rapidly cooled between the water cooled grips and retested within 10 minutes of achieving room temperature. The average elapsed time between the elevated temperature test and the low temperature test was 20 minutes. The specimens were strained to either 2% (1% at each temperature) or 4% (2% at each temperature) total strain. In addition to the Cottrell-Stokes tests, tension and compression tests were conducted at ambient temperature

on identical material to 4% total strain for comparison to the results of the Cottrell-Stokes tests.

4.3.3 Results and Discussion

The results of the three Cottrell-Stokes tests are presented as figure 4.6-4.8. In examining figure 4.6, note that the deformation is completely thermally reversible. This is an important result; it indicates that the deformation at the elevated temperature has virtually no effect upon the subsequent deformation at the lower temperature. This complete thermal reversibility is obviously consistent with the newly proposed model. However, this result is in conflict to the results of previous experiments conducted on single crystals on Ni_3Al which all showed some irreversibility [20,21,70]. In these latter tests, the upper test temperatures were closer to T_p ($T \geq 500°C$) and larger strains were applied (generally 2% at each test temperature). Figure 4.8 presents the data for a Cottrell-Stokes test run under identical temperature conditions to those in figure 4.6, but in this case to a higher strain level. Here the flow stress of the material is slightly increased (10%) by the previous deformation at the elevated temperature. The amount of increase corresponds to the degree of hardening experienced during deformation at 400° C.

When performing Cottrell-Stokes experiments with temperatures closer to T_p (600°C), the flow stress is also raised when retested at ambient temperature. Here the observed irreversibility can be attributed to dislocations present on cube slip planes. Although 600°C is below T_p, there is sufficient thermal activation to permit some primary cube glide although octahedral slip is still dominant. Since these dislocations are present on non-close packed planes, they require significant thermal activation to overcome the large Pierels

stresses. At ambient temperature, these dislocations become sessile from the lack of thermal activation and thus impede further glide on the favored octahedral system.

To summarize the results of the three Cottrell-Stokes tests, deformation in polycrystalline Ni_3Al exhibits full thermal reversibility under the following conditions:

(1) Low (<1%) total strains before significant hardening accumulates.

(2) Temperatures where primary cube slip can not operate.

If larger strains or temperatures are applied, the material demonstrates partial irreversibility. The amount of observed irreversibility was greatest when the elevated temperature deformation was close to T_p. Larger strains were also observed to increase the flow stress, but not nearly as dramatically as by elevating the temperature. The results of these experiments tend to support the current models predictions. At present it is uncertain whether any deformation process involving the thermally activated formation of KW locks can be consistent with thermal reversibility. If indeed KW locks occur by a thermally activated process, then a high density of such dislocations would be generated during the deformation at elevated temperature. These dislocations would then be present when retested at the lower temperature and give rise to the same flow stress level measured at the initial elevated temperature. Since this does not occur, there is a strong indication that if deformation in Ni_3Al is indeed controlled by KW locks, they must be much weaker obstacles to octahedral glide then previously envisioned. A second plausible explanation is that KW locks are an artifact of TEM investigations and as such are not a result of the deformation process.

5. CHARACTERISTICS OF MONOTONIC DEFORMATION

5.1 Experimental Procedures

Prior to tensile testing, all specimens were electro-polished in a solution of 80% methanol and 20% perchloric acid at -20° C using a current of 1.35 amps to eliminate machining defects. Following the electro-polishing procedure the diameter of all specimens were carefully measured to within 0.0254 mm. The tensile tests were conducted in the displacement control mode of an MTS servo-hydraulic test machine. The ramp rate was selected to achieve nominal strain rates of 10^{-2}/sec and 10^{-4}/sec during plastic deformation. These tests were conducted in both air and ultra-high vacuum ($< 10^{-8}$ MPa) environments. The vacuum environment was obtained in a Perkin-Elmore Vacuum chamber which was fitted to an MTS servo-hydraulic test machine. To obtain the ultra-high vacuum, two cryo-absorption pumps were used to achieve a vacuum of $< 10^{-4}$ MPa, then a compressed helium cryogenic pump was engaged to achieve the ultra-high vacuum levels utilized during testing. Elevated temperature (300° and 600° C) in the air environment was accomplished by heating the specimen and load train in a three-zone resistance furnace. In vacuum, the specimens were heated by a circular dense alumina single zone resistance heater with exposed elements which surrounded the specimen and portions of the load train in the vacuum chamber (figure 5.1). Specimen temperature was measured by one (air) or three (vacuum) type K thermocouple placed into contact with the specimen surface. Specimens were allowed to equilibrate at temperature for 1 hr prior to testing. The three-zone furnace permitted control of the specimen temperature to within ± 1° C during testing in air, while the single zone furnace controlled the temperature to within ± 5°C in the vacuum environment.

The output signals from the load cell and ram displacement were recorded by analog X-Y recorder and computer data acquisition. Following testing the diameter of the failed specimen was remeasured in the vicinity of the fracture surface. The data was reduced to obtain 0.2% offset yield strength, ultimate strength, and elongation to fracture. As all specimens were observed to experience discontinuous yielding accompanied by the development of Lüders bands, the reported yield strength was taken as the average stress during Lüders band propagation at the 0.2% strain offset. The failure strain reported was determined from the relationship:

$$\epsilon_f = \ln(A_i/A_f) \tag{5.1}$$

where A_i, and A_f are the initial and final area of the sample.

5.2 Yield Behavior

In Figure 5.2 (a) the experimental data obtained from measurement of 0.2% offset yield strength as a function of temperature. These results indicate that the yield strength (figure 5.2 (a)) of all alloys increases with temperature, reaching a peak value beyond 600°C. The yield strength of the binary and ternary alloy with 10μm grain size are virtually identical. For both alloys, the yield strength is observed to be slightly higher when tested at a strain rate of 10^{-2}/sec then for 10^{-4}/sec. The effect is more pronounced at elevated temperatures (>300°C). The ternary alloy with 3.5μm grain size is observed to be approximately twice as strong as with the larger grain size. A Hall-Petch analysis of the yield data was conducted using the equation:

$$\sigma_{ys} = \sigma_o + k_y(d)^{-1/2} \tag{5.2}$$

provided values of k_y = 1525 MPa·$\mu m^{-0.5}$ and σ_o = 67 MPa for the ternary alloy (Ni-Al-Cr).

These values were compared to values of k_y = 740 MPa·$\mu m^{0.5}$ and σ_o = 184 MPa reported for binary Ni_3Al+B of similar stoichiometry (*i.e.* 76 At.% Ni and 24 At.% Al with 0.1 At.% B) and processing history (powder extruded) tested at identical strain rates [71]. These values correlate fairly well with the binary alloy which was measured to have a 10.2μm grain size (*i.e.* σ_y = 410 MPa measured vs 414 MPa calculated). The constant k_y provides a measure of the grain-boundary's resistance to the transmission of slip from one grain to the next, and is related to the stress concentration required to operate dislocation sources at or near grain boundaries in unyielded grains. The constant σ_o is the frictional stress of dislocations on their slip planes which can be related to the yield stress of single crystals by division of a Taylor factor (2.75). From this description it can be seen the Cr additions significantly impede slip transmission to adjacent grains, while weakening the lattice resistance to slip.

5.3 Ductility

Figure 5.2 (b) and 5.2 (c) reports the trends in failure strain verse temperature for air and vacuum environments respectively. The binary alloy (Ni-Al-B) was observed to possess a high elongation (≈50%) to fracture at ambient temperature which degraded with increasing temperature. Increasing the strain rate was observed to increase the failure strain significantly at elevated temperatures, but not at ambient temperature. Accompanying the degradation in ductiiity was a gradual change in fracture mode (figure 5.3 (c) and (d)) from completely transgranular at ambient temperature to completely intergranular at 600° C. When examining the tensile behavior of the alloys tested in vacuum, there was no such

degradation in the failure strain and fracture surfaces were completely transgranular. Such behavior is consistent with dynamic embrittlement of the grain boundaries by oxygen at elevated temperature [4].

Examination of this same data for the ternary alloys (Ni-Al-Cr-B) with 3.5μm and 10.1μm grain size reveals that in both cases the ductility is lower than that of the binary alloy at ambient temperature, but is superior at elevated temperatures. The reduction at ambient temperature is accompanied by a very different fracture morphology (figure 5.3 (a) vs 5.4 (a)). Fracture in the binary alloy is transgranular while the fracture surfaces of the ternary alloy are completely intergranular. This observation can be related to the presence of weak grain boundaries in the ternary alloys. The increased resistance to slip transmission also increases the tendency for low enery intergranular fracture by raising the grain boundary stress. The combination of these two properties results in intergranular fracture and a reduced ductility.

Examination of the results of the tensile tests conducted in the vacuum environment (figure 5.2 c) reveal that although there is a very strong influence of environment on the failure strain of the binary alloy, there is only a very slight reduction for the ternary alloy. The Cr additions in the ternary alloy have effectively reduced if not eliminated environmental embrittlement at elevated temperature. One likely mechanism for the observed superiority of the ternary alloy is that the presence of Cr promotes the formation of a dense tenacious Cr_2O_3 oxide which protects the grain boundaries from environmental attack by reducing boundary diffusivity.

Comparison of the ductilities of the 10.2μm and 3.5μm grain size ternary alloys

reveals that the larger grain size increases the ductility at low temperatures ($T < 0.5\ T_m$). This behavior is in direct contrast to the behavior of binary alloys where grain refinement increases the ductility at both ambient and elevated temperatures [73,74]. There, the observed results were explained from the viewpoint of reducing the critical crack size present within the alloys and reduction in grain boundary stress from slip band pile ups at grain boundaries. In the ternary alloys with Cr, the observed behavior is interpreted to be consistent with difficulty of slip transmission across grain boundaries. The larger grain size imparts a higher average dislocation path length which imparts higher ductility in a material in which slip transmission across grain boundaries is difficult. In addition, examination of figure 5.4 (a) and (b) reveals significant differences in the appearance of intergranular fracture at ambient temperature between the two grain sizes. In the large grain size material, the grain boundary facets are decorated with particles. Such particles have been observed at the grain boundaries of similar intermetallic alloys [72] and were identified as chromium borides by microdiffraction analysis.

These particles were only rarely observed on the fracture surface of the small grain size material and their size was considerably smaller. The site preference of the particles indicates that nucleation was heterogeneous, and occurred during elevated temperature processing. These particles can be expected to exert a Zener drag force on the advancing boundary (which explains the relatively slow kinetics of grain growth in the Cr alloyed material with respect to the binary material). The elevated temperature processing to increase the grain size can be expected to both nucleate additional particles, and grow existing particles to larger sizes. As B and Cr both seggregate to the particles and away from

interstitial sites in the grain boundaries, these particles can reduce the grain boundary strength. The role of these particles on both ambient and elevated temperature deformation and crack growth will be examined more thoroughly in subsequent discussions.

At 600°C ($T > 0.5\ T_m$), the failure strains of the two alloys are virtually identical. This can be explained on the basis that as temperature increases the effectiveness of grain boundaries in impeding slip is reduced due to thermal activation. In this situation the ductility of the two grain sizes should converge in the absence of dynamic embrittlement and grain boundary sliding. Grain boundary sliding has been reported to significantly reduce the ductility of binary alloys with large grain sizes ($\approx 40\mu m$) at temperatures as low as 400° C [73,74]. Comparison of the fracture surfaces for the two different grain size ternary alloys at 600° (figure 5.4 (c) and (d)) indicates that significant plasticity occurs at the grain boundaries in the case of the large grain size material. Enhanced mechanical locking of the boundaries by the chromium boride particles reduces the tendency to form wedge cracks and provides the observed grain size independent ductility.

6. CHARACTERISTICS OF CYCLIC DEFORMATION

6.1 Experimental Procedures

Prior to low cycle fatigue testing all specimens were electro-polished using similar conditions as for the tensile specimens to remove machining defects. Prior to fatigue testing, translational (two perpendicular directions) and rotational alignment of the load train was achieved to within 0.0254 mm. This was accomplished to minimize bending moments and guarantee a uniform stress state within gauge section of the specimen. Low cycle fatigue testing was conducted in plastic strain control mode utilizing a SATEC CATS servo-hydraulic test machine. Elongation at both ambient and elevated temperature was measured using a MTS displacement gauge attached to alumina rods spring loaded onto the specimen. Plastic strain control was obtained using the combinatorial feedback output of the machine and the relationship:

$$\epsilon_p = \epsilon_t - P/A_o/E \qquad (6.1)$$

where

ϵ_t = strain conditioner output signal.
ϵ_p = plastic strain combinatorial output signal.
P = load conditioner output signal.
A_o = initial specimen diameter.
E = measured elastic modulus for current temperature.

Plastic strain control was obtained by generating total strain control ramps which were programmed to end on desired plastic strain output signals (typically $\epsilon_p = \pm 0.003$). Upon attaining the plastic strain endpoint of a given ramp, a sequencer was utilized to initiate a second total strain control ramp in the reverse sense. In this way a series of hysterisis loops could be generated with a constant loop width at zero stress regardless of hardening or softening characteristics.

Low cycle fatigue testing was conducted at temperatures of 25° and 600° C. Specimen heating was obtained by a Lepel 1200 Watt induction heater utilizing a well calibrated coil. The coil was adjusted to repeatedly obtain a temperature gradient of $\pm$ 5° C in the gauge section of a calibration specimen. During fatigue testing, specimen temperature was controlled by an Omega PID controller from thermocouples spot welded to the upper and lower shoulders. Shoulder temperature was chosen to correlate to the desired temperature distribution in the gauge section of the specimen. During elevated temperature testing the grips were water cooled. Specimens were equilibrated at temperature for 30 minutes prior to fatigue testing to ensure uniform heating throughout the gauge section of the specimen.

During fatigue testing, output signals of the load cell and displacement gauge were monitored using an analog strip chart recorder which continuously recorded the endpoints of each hysterisis loop. The output signals of the load cell, displacement gauge and combinatorial feedback channels were recorded by both analog X-Y recorder and computer data acquisition. This was conducted during selected fractions of the total fatigue life of the specimen.

Plastic strain ranges were selected to provide specimen life between 100 and 10000 cycles (ranging from 0.3% to 0.6%). In most cases the specimens failed suddenly without any prior tensile load drop. Initial tests were conducted to failure. Subsequent testing was also conducted under identical conditions then interrupted at life fractions where significant changes in the deformation response had previously occurred. The surfaces from these interrupted tests were replicated. The specimens were subsequently sectioned for TEM

microscopy to determine the evolution of cyclic damage during low cycle fatigue testing.

6.2 Deformation at 25°C

Figure 6.1 shows the cyclic hardening behavior for $\Delta\epsilon_p$ = 0.006 at ambient temperature for the binary and ternary alloys tested at 10^{-2}/sec. From this it can be seen that the characteristics of deformation of the binary and ternary alloy with 10μm grain size are very similar. During cyclic deformation, cyclic hardening was rapid, achieving a peak value (≈300% higher than the initial stress) followed by gradual softening. In the ternary alloy with a 3.5μm grain size, significant hardening is also observed, but failure occurs prior to achieving a peak value.

6.2.1 Cyclic Hardening

TEM investigation of samples interrupted in the regime of cyclic hardening (figure 6.2) revealed several types of dislocations. These were (1) APB coupled screw dislocations with **b** = <110>, (2) Mixed and edge dipoles with **b** = <110> on {111} planes, and (3) Faulted dislocations. The latter were observed to increase in density of with increasing accumulated plastic strain (figure 6.6), until at peak hardening reaching such large densities that separation of individual defects was difficult if not impossible. These dislocations were observed to be homogeneously distributed throughout all grains, predominantely on the primary <110>{111} slip system (as determined from Schmid factor analysis). Using standard BF and DF techniques for defect analysis [75] the faults were determined to be intrinsic in nature with a fault vector **R** = {111}. Utilizing the invisibility criterion the dislocations bounding the fault were both **b** = <121>. Trace analysis indicated the faulted

loops to be oriented along <110> directions. From these investigations the defects were characterized as SISF loops residing on the octahedral glide plane.

SISF loops have been observed in Ni_3Al deformed at low to intermediate temperatures [10,19,20,21,22,75]. At present the role of such dislocations in deformation is presumed to be minimal as they possess a highly non-planar core structure [6] and are presumed to be sessile. Until now there has been no reported observation of such loops resulting in cyclic hardening of Ni_3Al, although it has been recognized that such loops could serve as barriers to the glide of the a/2<110> screw dislocation [22].

These dislocations arise from one of two mechanisms; (1) dissociation of unit superdislocation into two a/3<112> partials [7] (using the notation of Thompson's tetrahedron);

$$\mathbf{2AB} \rightarrow \mathbf{2A}\delta + 2\delta\mathbf{B} \qquad (6.2)$$

or (2) shear dissociation of a/2<110> superpartial dislocations via the reaction [22];

$$<110> \rightarrow a/2<110> + a/2<110> \rightarrow a/6<110> + a/6<112> + a/3<112> \qquad (6.3)$$

which is energetically unfavorable in terms of self energy, but is realistic when considering that the a/3<112> partial is subjected not only to the attractive forces of both the Shockley partial and the SISF, but also to the repulsion of the a/2<110> partial. For the first mechanism to occur, it has been demonstrated that the ratio of the APB energy to SISF energy must be sufficiently large (in the range 25-35) [6,8]. For the second mechanism to occur, the APB/SISF energy ratio must be 10 [22]. For the range of APB and SISF energies observed (105-130 mJm^{-2} and 5 - 15 mJm^{-2}) [16,21] and predicted (140 mJm^{-2} and 13mJm^{-2}) [78] for Ni_3Al, the later mechanism is more favorable. Direct observation of this mechanism

was accomplished during in-situ deformation in the TEM [77]. Such dislocations were observed to nucleate from a/2<110> screw superpartial which had become pinned locally under the influence of an applied stress.

It is proposed that during cyclic deformation of the substoichiometric polycrystalline Ni_3Al alloys, cyclic deformation results in glide of a/2<110> APB coupled dislocations in screw orientation. Intersection of these dislocations on intersecting glide planes leads to the formation of dipoles and SISF bound dislocation loops. As the density of the sessile SISF loops on the octahedral glide planes increases, the induced strain field interacts with glissile dislocations resulting in higher stresses required to achieve the imposed plastic strain. As cycling continues, the density of the loops increases resulting in the observed hardening.

6.2.2 Cyclic Softening

As was previously described, rapid hardening to a peak value was followed by cyclic softening. Although observed in a variety of precipitate hardened materials, cyclic softening is not typically observed in homogeneous single phase materials (in the absence of sufficient thermal activation to allow recovery). Coincident with the occurrence of cyclic softening was the appearance of slip traces on specimen surfaces (figure 6.3). These slip traces were observed to increase in number with increased plastic work, becoming more closely spaced, at times resulting in microcracks. In the TEM, the slip bands were observed to exist within a background of SISF loops (figure 6.4). The SISF loops are observed to be oriented in <110> directions consistent with the primary slip system. The slip bands are aligned in <110> directions on {111} planes, which were generally not the primary active slip systems for the given grain (*i.e.* not highest Schmid factor). Slip bands were observed to nucleate

additional slip bands in adjacent grains (figure 6.4 (b)). At larger amounts of cyclic work, the slip band spacing decreases and occurs on intersecting <110>{111} slip systems (figure 6.4 (c)). Within these slip bands no SISF loops were observed, although the dislocation density is higher than that in the surrounding matrix.

It is proposed that once a critical density of SISF loops has accumulated during cyclic hardening, slip on the primary octahedral slip system requires a higher shear stress than that necessary to cause glide on the secondary octahedral slip system (due to a lower density of barriers). The slip bands are paths of least resistance for gliding dislocations. Where these slip bands intersect grain boundaries, the increased stress resulting from the dislocation pile ups nucleates additional slip bands. As cycling continues, the number of slip bands increases. These slip-bands through the heavily work-hardened matrix apear to be similar to persistant slip bands (described by Laird for single phase metals) in which deformation occurs more easily.

6.3 Cyclic Deformation at 600° C

At elevated temperatures, the characteristics of cyclic deformation were quite different than at ambient temperature. The materials behaved quite differently for different strain rates unlike at ambient temperature where the deformation response and substructures were similar. During cyclic deformation both creep and environmental attack were found to play a significant role in determining the life at a given plastic strain range.

Figure 6.5 indicates the cumulative glide behavior of the alloys at a strain rates of 10^{-2}/sec and 10^{-4}/sec. When tested at 10^{-2}/sec, all materials hardened significantly, while when tested at the lower strain rate (10^{-4}/sec) the materials all soften significantly. The

ability of both materials to absorb plastic work was found to be at least an order of magnitude higher for the lower strain rate. This effect was particularly pronounced for the binary alloy in which the life increased by 3 orders of magnitude when strained at a rate of 10^{-4}/sec. As could be expected from the results of the tensile tests (section 4), the cyclic stress amplitude for a given plastic strain was higher for the 10^{-2}/sec strain rate.

In all cases, crack initiation and propagation occurred by intergranular fracture. Slip traces were not observed on the specimen surfaces. TEM observations of the deformation substructures of the alloys at the two different strain rates (figure 6.6) reveal very different deformation characteristics between the two strain rates.

The predominant features of the deformation substructures at 600° C were homogeneous distributions of long straight a/2<110> screw dislocations. Although isolated SISF loops were observed, the density of these dislocations was insufficient for wither deformation or hardening. The virtual absence of such faults is consistent with previous observations of SISF loops [19-22]. In one of these studies, it was proposed that the increased thermal activation permits recombination of the a/3<121> partials [22]. At the higher strain rate the density of dislocation debris was considerably higher. The dislocation debris was in the form of mixed a/2<110> loops and dipoles resulting from the intersection of the glissile dislocations. When tested at a rate of 10^{-4}/sec, the deformed material contained a much lower density of dipoles, and relatively no loops or defect clusters. An additional feature of the deformation substructure when tested at the lower strain rate is considerable bowing of predominantly screw oriented dislocations in the cube plane. Figure 6.7 (a) is a weak-beam photomicrograph taken with the the beam direction **B** = [010] which

indicates examples (arrows) of bowed dislocations. Bowing of screw dislocations onto cube planes at elevated temperature has been correlated to non-conservative creep deformation in Ni_3Al [70]. In addition, dislocation networks (figure 6.7 (b)) were observed at the grain boundaries of specimens tested at the lower strain rate.

These observations indicate that at 600° C, deformation again occurs from the motion of a/2<110> APB bound screw dislocations. Intersection of these dislocations during reversed loading leads to the formation of dislocation debris in the form of defect clusters, loops and dipoles. This debris interferes with the movement of the glissile dislocations, with continued cycling results in significant cyclic hardening. At the lower strain rate, the dislocation density remains relatively low as the defects are either swept to the grain boundaries, or migrate to the glissile dislocations. In addition, there is considerable evidence for thermally activated glide of these dislocations on cube planes. The combination of these two mechanisms results in the observed softening observed during elevated temperature cyclic deformation.

Failure occurs at lower levels of plastic work in the harder (10^{-2}/sec) material due to higher stress levels that enhance dynamic embrittlement of the grain boundaries. The dynamic embrittlement mechanism is thus responsible for crack nucleation. When tested at the lower strain rate, cycling results in softening and crack nucleation is consequently delayed.

7. FATIGUE CRACK PROPAGATION

7.1 Experimental Procedures

Prior to fatigue crack propagation, the specimens were ground and polished. The final polishing was conducted with 1μm diamond paste. Following polishing, stainless steel resistance leads were welded onto the specimens. Fatigue loading was conducted in the load control mode of a MTS servo-hydraulic test machine in both air and ultra-high vacuum ($< 10^{-9}$ MPa) environments. The vacuum environment was obtained in the vacuum chamber described in Chapter 4. An R-ratio (K_{min}/K_{max}) of 0.1 was utilized for all tests. Test frequency was 10 Hz. Cracking was initiated in the near threshold regime.

Testing was conducted at temperatures of 25° and 600° C. The elevated temperatures were obtained in air by heating the specimen and portions of the load train in a three zone resistance furnace. Specimen temperature was measured by two type K thermocouples spot welded onto the specimen slightly below the anticipated plane of cracking. In vacuum, a rectangular, single zone dense ceramic resistance heater with exposed elements was used to heat the specimen (figure 7.1). It was determined that this specimen to heater geometry induced a temperature gradient of 20° C across the anticipated path of crack growth. Three type K thermocouples were spot welded onto the specimens directly below the anticipated plane of cracking. During testing, the furnace temperature was adjusted to provide the desired temperature at the current location of the crack tip to within $\pm$5° C.

Crack length was continuously monitored by dc potential drop method. Data was recorded using analog strip chart recorders and via computer data acquisition. The

technique was initially calibrated from visually monitoring crack length during testing with travelling microscopes. Precracking of all specimens was conducted in the temperature/environment in which the actual test was to be conducted.

At ambient temperature, crack closure was evaluated utilizing a technique developed in the MPRL laboratory [79]. A Zygo laser extensometer with 10^{-8} mm resolution was focused onto the machine slot at the load line of the compact test specimens. Prior to closure measurements, a linear output from the apparatus was obtained from an uncracked specimen. The results of these measurements revealed that the measured closure loads were typically lower than P_{min}. Thus closure mechanisms did not alter test results.

7.2 Results at Ambient Temperature

The results from the fatigue crack propagation testing in air are presented in figure 7.2. These results indicate that the fatigue crack growth resistance (FCGR) of the binary alloy is greater than that of the ternary alloy. The FCGR of the ternary alloy with the smaller (3.5μm) grain size less than that with the 10.2μm grain size by over an order of magnitude. The difference between crack growth rates for the binary (Ni-Al + B) and ternary (Ni-Al-Cr + B) alloy with identical grain sizes was over 3 orders of magnitude. The reproducibility of data was confirmed with the large grain size ternary alloy.

Crack growth in the binary alloy was observed to occur by transgranular fracture. Planar slip deformation was revealed from the highly crystallographic facets (figure 7.3 (a)). Such morphology is characteristic of a material experiencing planar slip consistent with the deformation observations (section 6.2.2). The crack path in the ternary alloy was observed

to be predominantly intergranular for both grain sizes (figure 7.3 (b) and (c)). The fracture surface of the smaller grain size ternary material was observed to have 30%-50% transgranular crack growth (figure 7.3 (b)) (indicates planar slip deformation). The areal fraction of intergranular fracture increased with increasing ΔK. The fracture surfaces of the ternary alloy with the large grain size were observed to be completely intergranular (figure 7.3 (c)). The grain boundaries in both alloys were observed to possess numerous parallel ledges from emergence of active slip planes.

These observations were interpreted to be consistent with the prior mechanical behavior (tensile and LCF). The grain boundaries in the binary alloy are stronger (greater cohesive strength) and better able to initiate/transfer slip in/to adjacent grains than for the ternary alloys. Between the large and small grain sizes in the ternary alloy, the smaller grain size had stronger grain boundaries. Chromium-boride precipitates observed on the fractured grain boundaries of the material with the 10.1μm indicate weakening by B depletion. This weakening subsequently enhances crack growth as intergranular fracture absorbs far less work than transgranular fracture. In intergranular fracture, the applied normal stress exceeds the grain boundary cohesive strength allowing for crack propagation. Variation in the grain boundary cohesive strength will result in different intergranular crack growth rates. For these reasons, the observed differences in FCGR are correlated to ratio of transgranular to intergranular crack growth.

6.3 Crack Growth at 600°

At elevated temperatures, the crack growth rates increase substantially for all alloys

(figure 7.4). The crack growth resistance of the ternary alloy at elevated temperature is greater than that of the binary alloy (figure 7.5). The crack growth resistance of the binary alloy decreases by over 5 orders of magnitude from that possessed at room temperature. In vacuum (figure 7.6), the crack growth rate increases by 2 orders of magnitude (3 orders of magnitude smaller than the rate measured in air). These results are accompanied by differences in crack path. In air, the material cracks along the grain boundaries, but in vacuum the fracture morphology is predominantly transgranular (figure 7.7). These results indicate that oxygen diffusion along grain boundaries in the presence of an applied stress field results in reduction of grain boundary cohesive strength. These observations indicate that environmentally assisted crack growth controls the temperature dependence of the FCGR of the binary alloy.

Examination of the results for the ternary alloy reveals an order of magnitude increase in crack growth rate from that observed at ambient temperature (figure 7.4 (a) and (b)). The increase was greatest for the smaller grain size material. The fracture surfaces were almost completely intergranular in both cases (figure 7.8). Once again, the crack growth resistance of the 10.1μm grain size material was lower than that with a 3.5μm grain size. The difference in these rates is attributed to a lower grain boundary cohesive strength in the 10.1μm material caused by the growth of chromium boride particles. These results indicate that environmental attack does occur along the grain boundaries, but it has a lower influence upon the crack growth rate in the C. alloys.

8. CONCLUSIONS

1. An analytical examination of the kinetics of thermally activated strengthening during deformation of Ni_3Al indicated that they are sufficiently rapid to give rise to an equilibrium substructure in time intervals much less than those associated with normal strain rates.

2. This concept was used to demonstrate the strain rate independence of Ni_3Al alloys and develop a model based upon thermodynamic considerations for yielding in Ni_3Al. The model prdicts all experimental observations for Ni_3Al.

3. For the model to predict the increase in strength with temperature, a positive driving force for cross-slip is required.

4. Experimental observations of complete thermal reversibility were made and used to provide additional justification for the theoretical model.

5. The degree of thermal reversibility was experimentally demonstrated to be a function of prior strain and deformation temperature. The higher the temperature or strain, the less the reversibility.

7. The yield strength of the binary and ternary alloys was found to be virtually identical for

similar grain size, stoichiometry and temperature.

8. A Hall-Petch analysis indicated that Cr additions increase the difficulty of slip transmission between adjacent grains while decreasing the lattice resistance to slip relative to binary alloys.

9. Cr additions resulted in the nucleation and growth of chromium boride precipitates at the grain boundaries of Ni_3Al alloyed with 8 at.% Cr and 0.25% B during elevated temperature processing.

10. Chromium boride precipitates degrade the grain boundary cohesive strength by a reduction in the boron concentration at the grain boundaries.

11. Cyclic deformation of Ni_3Al occured by planar slip, at times resulting in the formation of persistent slip bands which led to softening.

12. An increasing density of dislocations on the slip bands increases both slip band and grain boundary stress. This results in either transgranular or intergranular crack initiation depending upon the grain boundary strength.

13. Diffusion of gaseous oxygen aided by crack tip stress fields was demonstrated to control high temperature deformation properties by degradation of the grain boundary cohesive

strength.

14. At elevated temperature, Cr decreases the rate of environmental attack along the grain boundaries.

REFERENCES

1. K. Aoki and O. Izumi, "On the Ductility of the Intermetallic Compound Ni_3Al", *Nippon Kinzoka Gakkaishi*, 1979, vol. 43, p. 1190.

2. R.G. Davies and N.S. Stoloff, "On the Yield Stress of Aged Ni-Al Alloys", *Transactions of the Metallurgical Society of AIME*, 1965, vol. 233, p. 714.

3. C.T. Liu, C.L. White and J.A. Horton, "Effect of Boron on Grain-Boundaries in Ni_3Al", *Acta Metallurgica*, 1985, vol. 33, p. 213.

4. A.I. Taub, K.M. Chang and C.T. Liu, "Effects of Environment on the Elevated Temperature Ductility of Boron-Doped Ni_3Al","Nickel Aluminides for Structural Use", *Scripta Metallurgica*, 1986, vol. 20, p. 1613.

5. C.T. Liu and V.K. Sikka, "Nickel Aluminides for Structural Use", *Journal of Metals*, 1986, vol. 38, p. 19.

6. V. Paidar , M. Yamaguchi, D.P. Pope and V. Vitek, "Dissociation and Core Structure of <110> Screw Dislocations in $L1_2$ Ordered Alloys-II. Effects of Applied Shear Stress", *Philosophical Magazine A*, 1982, vol. A45, p. 883.

7. B.H. Kear, A.F. Giamei, J.M. Silock and R.K. Ham, "Slip and Climb Processes in γ' Precipitation Hardened Nickel-Base Alloys", *Scripta Metallurgica*, 1968, vol. 2, p. 287.

8. M. Yamaguchi, V. Paidar, D.P. Pope and V. Vitek, "Dissociation and Core Structure of <110> Screw Dislocations in $L1_2$ Ordered Alloys-I.Core Structure in an Unstressed Crystal", *Philosophical Magazine A*", 1982, vol.A45, p. 867.

9. T.A. Parthasarathy, D.M. Dimiduk, D. Woodward, and D. Diller, "Computer Simulation of a_o<110> Screw Dislocations in Ni3Al", To be Published in J.O. Stiegler, D.P. Pope, C.T. Liu editors High-Temperature Ordered Intermetallic Alloys IV, Materials Research Society.

10. S. Takeuchi and E. Kuramoto, "Temperature and Orientation Dependence of the Yield Stress in Ni_3Ga Single Crystals",
Acta Metallurgica, 1973, vol. 21, p. 415.

11. C. Lall, S. Chin and D.P. Pope, "The Orientation and Temperature Dependence of the Yield Stress of $Ni_3(Al,Nb)$ Single Crystals", *Metallurgical Transactions A*, 1979, vol. 10A, p. 1323.

12. V. Paidar, D.P. Pope and V. Vitek, "A Theory of the Anomalous Yield Behavior in $L1_2$ Ordered Alloys", *Acta Metallurgica*, 1984, vol. 32, p.435.

13. P.A. Flinn, "Theory of Deformation in Superlattices", *Transactions of the Metallurgical Society of AIME*, 1968, vol. 218, p. 145.

14. P.H. Thorton, R.G. Davies, and T.L. Johnston, "The Temperature Dependence of the Flow Stress of the γ' Phase Based Upon Ni_3Al", *Metallurgical Transactions*, vol. 1, 1970, p.207.12.

15. Y.Q. Sun and P.M. Hazzledine, "A TEM Weak-Beam Study of Dislocations in γ' in a Deformed Superalloy", *Philosophical Magazine A*, 1988, vol. A58, p. 603.

16. P. Véyssiere, J. Douin and P. Beauchamp, "Observations of Dislocations in Ni_3Al", *Philosophical Magazine A*, 1985, vol. A53, p. 469.

17. P. Veyssiere, "Transmission Electron Microscope Observation of Dislocations in Ordered Intermetallic Alloys and the Flow Stress Anomaly", In C.T. Liu and A.I. Taub and N.S. Stoloff and C.C. Koch editors High Temperature Ordered Intermetallic Alloys III, Materials Research Society, 1989, p. 175.

18. M. A. Crimp, "HREM Examination of [101] Screw Dislocations in Ni_{3Al}", *Philosophical Magazine Letters*, 1989, vol. 60, p. 45.

19. I. Baker and E.M. Schulson, "The Effect of Temperature on Dislocation Structures in Ni_3Al", *Physical States of Solids (a)*, 1985, vol. 89, p.163.

20. D. Dimiduk, "Strengthening by Substitutional Solutes and the Temperature Dependence of the Flow Stress in Ni_3Al", WRDC-TR-89-4106, 1989.

21. W.E. Dowling, Oxidation and Its Influence on the Mechanical Behavior of Ni_3Al, Ph.D. dissertation, University of Michigan-Ann Arbor, 1989.

22. P. Véyssiere, J. Douin, and P. Beauchamp, "On the presence of superlattice intrinsic stacking faults in plastically deformed Ni_3Al", *Philosophical Magazine A*, 1985, vol. 51, p. 469.

23. R. A. Mulford and D.P. Pope, "The Yield Stress of $Ni_3(Al,W)$", *Acta Metallurgica*, vol. 21, 1973, p. 1375.

24. Y. Mishima, Y. Oya, T. Suzuki, "Characteristic Mechanical Properties and Phase Stability of $L1_2$ Intermetallic Compounds", In C.C. Koch, C.T. Liu, and N.S. Stoloff editors, High Temperature Intermetallic Alloys, 1985, Materials Research Society, p. 227.

25. T. Suzuki, Y. Mishima, S. Miura, "Plastic Behavior in $Ni_3(Al,X)$ Single Crystal-Temperature, Strain Rate, Orientation, and Composition, *ISIJ International*, vol. 29, 1989, 1, p.1.

26. B.A. Greenberg, M.A. Ivanov, Y.N. Gornostirev, and L.E. Karkina, "Phenomenalogical Theory of Plastic Deformation with Several Types of Mobile and Immobile Dislocations II. An Analysis of the Features of Plastic Deformation of Ordered Alloys With a Superstructure $L1_2$", *Physical States of Solids A*, vol. 49, 1978, p. 517.

27. B.A. Greenberg, M.A. Ivanov, YU.N. Gornostryrev, and L.E. Karkina, *Physical States of Solids A*, vol. 38, 1976, p. 653.

28. P.M. Hazzledine, M.H. Yoo, and Y.Q. Sun, "The Geometry of Glide in Ni_3Al at Temperatures Above the Flow Stress Peak", *Acta Metallica*, vol. 37, 12, p.3255.

29. T. Ogura, S. Hanada, T. Masumoto and O. Izumi,"Grain Boundary Fracture of $L1_2$ Type Intermetallic Compound Ni_3Al", *Metallurgical Transactions A*, vol. 16A, 1985, p. 441.

30. A.I. Taub and C.L. Briant, "Grain Boundary Chemistry and Ductility in Ni-Base $L1_2$ Intermetallic Compounds", In N.S. Stoloff and C.C. Koch and C.T. Liu and O. Izumi editors High Temperature Ordered Intermetallic Alloys II, Materials Research Society, 1987, 343.

31. O.Izumi and T. Takasugi, "Deformability Improvements of $L1_2$-Type Intermetallic Compounds", In N.S. Stoloff and C.C. Koch and C.T. Liu and O. Izumi editors High Temperature Ordered Intermetallic Alloys II, Materials Research Society, 1987, p. 173.

32. C.L. White and A. Choudhury,"Grain Boundary and Surface Segregation in Boron Doped Ni_3Al", In N.S. Stoloff, C.C. Koch, C.T. Liu, and O. Izumi editors High Temperature Ordered Intermetallic Alloys II, Materials Research Society,
1987, p.427.

33. J.A. Horton, M.K Miller, C.T. Liu, E.P. George and J.Bentley, "Effect of Aluminum Level on Boron Clustering in Ni_3Al", In C.T. Liu and A.I. Taub and N.S. Stoloff and C.C. Koch editors High Temperature Ordered Intermetallic Alloys III, Materials Research Society, 1989, p. 89.

34. D.D. Sieloff, S.S. Brenner and M.G. Burke, "FIM/Atom Probe Studies of B-Doped and Alloyed Ni_3Al", In N.S. Stoloff and C.C. Koch and C.T. Liu and O. Izumi editors High Temperature Ordered Intermetallic Alloys II, Materials Research Society, 1987, p. 87.

35. D.N. Sieloff, S.S. Brenner and H. Ming-Jian,"The Microchemistry of Grain Boundaries in Ni_3Al", In C.T. Liu and A.I. Taub and N.S. Stoloff and C.C. Koch editors High Temperature Ordered Intermetallic Alloys III, Materials Research Society, 1989, p. 155.

36. H.G. Bohn, J.M. Williams, J.H. Barrett, and C.T. Liu, "Lattice Location of Boron and Hafnium Dopants in an Ordered
Nickel Aluminide by use of Ion Channeling/Nuclear Reaction Analyses", In N.S. Stoloff and C.C. Koch and C.T. Liu and O. Izumi editors High Temperature Ordered Intermetallic

Alloys II, Materials Research Society, 1987, p. 127.

37. E.M. Schulson, T.P. Weihs, I. Baker, H.J. Frost, and J.A. Horton, "Grain Boundary Accommodation of Slip in Ni_3Al Containing Boron", *Acta Metallurgica*, vol. 34, 1986, p. 1395.

38. V. Vitek, S.P. Chen, A.F. Voter, J.J. Kruisman and J.Th.M. DeHosson, "Grain Boundary Structure and Intergranular Fracture in $L1_2$ Ordered", *Materials Science Forum*, vol. 46, 1989, p. 237.

39. S.P. Chen, A.F. Voter, R.C. Albers, A.M. Borin and F.J. Hay, "Theoretical Studies of Grain Boundaries in Ni_3Al with Boron or Sulfur", *Scripta Metallurgica*, vol. 23, 1990, p. 2061.

40. T. Takasugi and O. Izumi, "Electronic and Structural Studies of Grain Boundary Strength and Fracture in $L1_2$ Ordered Alloys-I.
Binary A_3B Alloys", *Acta Metallurgica*, vol.33, 1985, p. 1247.

41. A.H. King and M.H. Yoo, "Dislocation Reactions at Grain Boundaries in $L1_2$ Ordered Alloys", In N.S. Stoloff and C.C. Koch and C.T. Liu and O. Izumi editors High Temperature Ordered Intermetallic Alloys II, Materials Research Society, 1987, p. 99.

42. C.T. Liu, C.L. White, and E.H. Lee, "Effect of Test Environment on Ductility and Fracture Behavior of Boron-Doped Ni_3Al at 600° C", *Scripta Metallurgica*, vol. 19, 1985, p. 1247.

43. M. Takeyama and C.T. Liu,"Effects of Grain Size and Test Temperature on Ductility and Fracture Behavior of a B-Doped Ni_3Al Alloy", *Acta Metallurgica*, vol. 36, 1988, 5, p. 1241.

44. M. Takeyama and C.T. Liu, " Effect of Preoxidation and Grain Size on Ductility of a Boron-Doped Ni_3Al at Elevated Temperatures", *Acta Metallurgica*, vol. 37, 1989, 10, p. 2681.

45. C.T. Liu anc C.L. White, "Dynamic Embrittlement of Boron-Doped Ni_3Al Alloys at 600° C, *Acta Metallurgica*, vol. 35, 1987, p. 643.

46. C.T. Liu and B.F. Oliver, "Effect of Grain Shape on Environmental Embrittlement in Ni_3Al Tested at Elevated Temperatures", *Journal of the Materials Research Society*, vol. 4, 1989, p. 294.

47. N.R. Bonda, D.P. Pope, and C. Laird, "Cyclic Deformation of $Ni_3(Al,Nb)$ Single Crystals at Ambient and Elevated Temperatures", *Acta Metallurgica*, vol. 35, 1987, 9, p. 2371.

48. L.M. Hsiung and N.S. Stoloff, "Electron Microscopy Study of Fatigue Crack Initiation in Ni_3Al", In C.T. Liu and A.I. Taub and N.S. Stoloff and C.C. Koch editors High Temperature Ordered Intermetallic Alloys III, Materials Research Society, 1989, p. 261.

49. S.S. Ezz and D.P. Pope, "The Asymmetry of Cyclic Hardening in $Ni_3(Al,Nb)$ Single Crystals", *Scripta Metallurgica*, vol. 19, 1985, p.741.

50. H. Pak, M. Kato and D.P. Pope, "Friction Stress and Back Stress in Cyclically Deformed Ni_3Ge Single Crystals", *Materials Science and Engineering*, vol. 100, 1988, p. 31.

51. N.R. Bonda, D.P. Pope and C. Laird, "The Dislocation Structures of $Ni_3(Al,Nb)$ Single Crystals Fatigued at Ambient and Elevated Temperatures", *Acta Metallurgica*, vol. 35, 1987, p. 2385.

52. D.D. Krueger, B.J. Marquardt and R.D. Field, "Structure and Properties of Powder Metallurgy Ni_3Al Alloys", In N.S. Stoloff and C.C. Koch and C.T. Liu and O. Izumi editors High Temperature Ordered Intermetallic Alloys II, Materials Research Society, 1987, p. 309.

53. K.M. Chang, S.C. Huang and A.I. Taub, "High Temperature Fatigue Crack Propagation in P/M Ni_3Al-B Alloys", In N.S. Stoloff and C.C. Koch and C.T. Liu and O. Izumi editors High Temperature Ordered Intermetallic Alloys II, Materials Research Society, 1987, p. 303.

54. N.S. Stoloff, G.E. Fuchs, A.K. Kuruvilla and S.J. Choe, "Fatigue of Intermetallic Compounds", In N.S. Stoloff and C.C. Koch and C.T. Liu and O. Izumi editors High Temperature Ordered Intermetallic Alloys II, Materials Research Society, 1987, p. 247.

55. W. Matuszyk, G. Camus, D.J.Duquette, and N.S. Stoloff, "Effects of Temperature and Environment on the Tensile and Fatigue Crack Growth Behavior of a Ni_3Al-Base Alloy", *Metallurgical Transactions A*, vol. 21A, 1990, p. 2967.

56. R.W. Guard and J.H. Westbrook, "Alloying Behavior of Ni_3Al (γ' Phase), *Transactions of the Metallurgical Society of AIME*, vol. 215, 1959, p. 807.

57. S.D. Antolovich and G. Webb, "Cyclic Deformation, Damage, and Effects of Environment in the Ni_3Al Ordered Alloy at Elevated Temperature", Progress Report for period 12-1-88 through 6-1-88, AFOSR-87-0162.

58. B.H. Kear and H.G.F. Wilsdorf, "Dislocation Configurations in Plastically Deformed Polycrystalline Cu_3Au Alloys", *Transactions of the Metallurgical Society of AIME*, vol. 224, 1962, p. 382.

59. V. Vitek, "From Dislocation Cores to High Temperature Strain Rate Effects in $L1_2$ Alloys", To appear in L. Johnson, J.O. Stiegler, and D.P. Pope editors High Temperature Ordered Intermetallic Alloys IV, Materials Research Society, vol. 213.

60. B.A. Greenberg and L.I. Yakovenkova, "Incomplete Cross-Slip of Superdislocations in Ordered Cu_3Au-Type Alloys", *Physical States of Solids A*, vol. 18, 1973, p. K129.

61. B.A. Greenberg and L.I. Yakovenkova, "Dislocation Barriers in Ordered Cu_3Au-Type Alloy", *Physical States of Solids A*, vol. 20, 1973, p. K53.

62. B.A. Grinberg, YU. N. Gornostryrev, and L.I. Yakovenkova, "Thermally Activated Transformations of Superdislocations in an Ordered Alloy of the Cu_3Au Type", *Physical Metal Metallurgica*, vol. 39, 1975, p. 960.

63. B.A. Greenberg and M.A. Ivanov,"On the Theory of Plastic Deformation with an Account of Dislocation Transformations of Several Types", *Physical States of Solids A*, vol. 45, 1978, p. 403.

64. B.A. Greenberg, M.A. Ivanov, YU.N. Gornostirev, and L.W. Karkina,"Phenomenological Theory of Plastic Deformation with Several Types of Mobile and Immobile Dislocations I.Theory", *Physical States of Solids A*, vol. 47, 1978, p.731.

65. Y.N. Gornostyrev, B.A. Grinberg, L.I. Yakovenkova, "Free Transformations of Superdislocations and Temperature Peculiarities of the Plastic Behavior of Ordered Alloys with $L1_2$ Structure", *Physica Metal Metallurgica*, vol. 51, 1981, 4, p. 170.

66. A. de Bussac, G. Webb, and S.D. Antolovich, "A Model for the Strain-Rate Dependence of Yielding in Ni_3Al Alloys", *Metallurgical Transactions A*, vol. 22A, 1991, p.125.

67. A. de Bussac, G. Webb, and S.D. Antolovich, "A Model for the Yield Behavior of Ni_3Al Alloys", To appear in L. Johnson, J.O. Stiegler, and D.P. Pope editors High Temperature Ordered Intermetallics IV, Materials Research Society. vol. 213.

68. S. Miura, S. Ochiai, Y. Oya, Y. Mishima and T. Suzuki, "Effect of Strain Rate on the Plastic Behavior of $L1_2$ Compounds Based on Ni_3Al", In C.T. Liu and A.I. Taub and N.S. Stoloff and C.C. Koch editors High Temperature Ordered Intermetallic Alloys III, Materials Research Society, 1989, p. 341.

69. J. Bonneville and J.L. Martin, "The Strain Rate Sensitivity of $Ni_3(Al,Ta)$ Single Crystals", To be published in L. Johnson, J.O. Stiegler and D.P. Pope editors High Temperature Ordered Intermetallic Alloys IV, Materials Research Society, vol. 213

70. K. Hemker, "A Study of the High Temperature Deformation of the Intermetallic Alloy Ni_3Al", Ph.D. Dissertation, Stanford University, 1990.

71. M. Takeyama and C.T. Liu, "Effect of Grain Size on Yield Strength of Ni_3Al and Other Alloys", *Journal of Material Research*, vol.4, 1988, p. 665.

72. C.A. Hippsley and J.H. DeVan, "Mechanisms of High Temperature Crack Growth in Nickel Aluminide", *Materials Science and Technology*, vol. 6, 1990, p. 93.

73. T.P. Weihs, V. Zinoviev, D.V. Viens and E.M. Schulson, "The Strength, Hardness and Ductility of Ni_3Al With and Without Boron", *Acta Metallurgica*, vol. 35, 1987, p. 1109.

74. E.M. Schulson, I. Baker, and H.J. Frost, "The Strength and Ductility of Intermetallic Compounds: Grain Size Effects", In N.S. Stoloff and C.C. Koch and C.T. Liu and O. Izumi editors High Temperature Ordered Intermetallic Alloys II, Materials Research Society, 1987, p. 195.

75. J.W. Eddington, Practical Electron Microscopy in Materials Science Vol 4. Defect Analysis and Characterization, Van Nostrand Reinhold Ltd., New York, 1976.

76. R. Bonnet and D. David, "Estimation des Energies de Fautes Intrinseques Dans des Phases (Ni, Al, Ti, Cr) Basees sur Ni_3Al", *Acta Metallurgica*, vol. 39, 3, 1991, p. 329.

77. PH. Lours, A. Coujou and B. De Mauduit, "On the High-Temperature Stress-Induced Spreading of Superlattice Intrinsic Stacking Faults in γ' Nickel-Based Single Crystals" *Philosophical Magazine A*, vol. 62, 2, 1990, p. 253.

78. S.P.Chen, A.F. Voter and D.J. Srolovitz, *Scripta Metallurgica*, vol. 20, 1986, p.1389.

79. R.R. Bowman, R.C. Brown, and S.D. Antolovich, "Problems Associated with Closure Load Determinations", *Engineering Fracture Mechanics*, vol. 33, 1988, p. 703.

PUBLICATIONS, PRESENTATIONS AND INTERACTIONS

I. PUBLICATIONS

1. A. de Bussac, G. Webb, and S.D. Antolovich, "A Model for the Strain-Rate Dependence of Yielding in Ni_3Al Alloys", *Metallurgical Transactions A*, vol. 22A, 1991, pp.125.

2. A. de Bussac, G. Webb, and S.D. Antolovich, "A Model for the Yield Behavior of Ni_3Al Alloys", To appear in L. Johnson, J.O. Stiegler, and D.P. Pope editors High Temperature Ordered Intermetallics IV, Materials Research Society.

3. A. de Bussac, G. Webb, and S.D. Antolovich, "A Model for Yielding in Ni_3Al", in preparation for submission to Metallurgical Transactions.

4. G.Webb and S.D. Antolovich, "Fatigue Response of Polycrystalline Ni_3Al Alloys", in preparation for submission to Metallurgical Transactions.

II. PRESENTATIONS

1. G. Webb and S.D. Antolovich, "An Investigation for the Fundamental Mechanisms of Cyclic Hardening in Ni_3Al", MRS Fall Meeting, Symposia Q, High Temperature Ordered Intermetallic Alloys, November 26 - December 1 1990, Boston, Massachusetts.

2. G. Webb and S.D. Antolovich, "Cyclic Deformation of Ni_3Al as a Function of Compostion, Temperature, and Strain Rate", Aeromat '90, May 5-8 1990, Long Beach, California.

3. G. Webb. S.D. Antolovich, and R.R. Bowman, "Fatigue Crack Propagation of Ni_3Al as a Function of Compositon and Temperature", TMS Annual Meeting and Exposition, February 19-22 1990, Anaheim, California.

4. G. Webb, S.D. Antolovich, and R.R. Bowman, "High Temperature Fatigue Response of Ni_3Al-Structure Property Relations", ASM-TMS Materials Week, October 2-5 1989, Indianapolis, Indiana.

III. INTERACTIONS

1. **OaK Ridge National Laboratory**, Dr. C.T. Liu was consulted prior to specification of alloy compositions, and he serves on the PhD committee of Mr. Webb. Several technical discussions have also been conducted with Dr. P.M. Hazzledine regarding TEM experiments and analytical modeling.

2. **Stanford University**, Dr. W.D. Nix visited Ga.Tech and had several discussions regarding the analytical modeling of anomolous yielding.

3. **NASA-Lewis Research Center,** Numerous technical discussions have been held with Dr. R.R. Bowman regarding TEM techniques employed during the course of the research. Dr. Bowman served as in a post-doctoral fellow on the project as was responsible for the specification of alloy compositions.

4. **Michigan Tech University,** Dr. W.W. Milligan visited Ga.Tech and demonstrated weak-beam imaging techniques.

IV. Personnal

All those who have participated on the project are listed below;

NAME	FUNCTION
1. Stephen D. Antolovich	Principal Investigator
2. Graham Webb	Ph. D. graduate student who carried out the bulk of experimental work and is in the process of writing Ph.D. dissertation.
3. Randy Bowman	Post-doctoral fellow. Specified the initial alloy compositions.
4. Rick Brown	Technician in the MPRL. Helped with testing and design of some experiments.
5. Pat Ledon	Senior administration secretary. Ms. Ledon administered some aspects of the project.
6. Others	Some assistance was obtained from secretaries, technicians and students in the School of Materials Engineering.

Table 3.1 Compositions of experimental alloys.

(ATOMIC PERCENT)

	Ni	Al	Cr	B
ALLOY B	76.3	23.5	0.0	0.2
ALLOY T	72.1	19.7	7.8	0.2

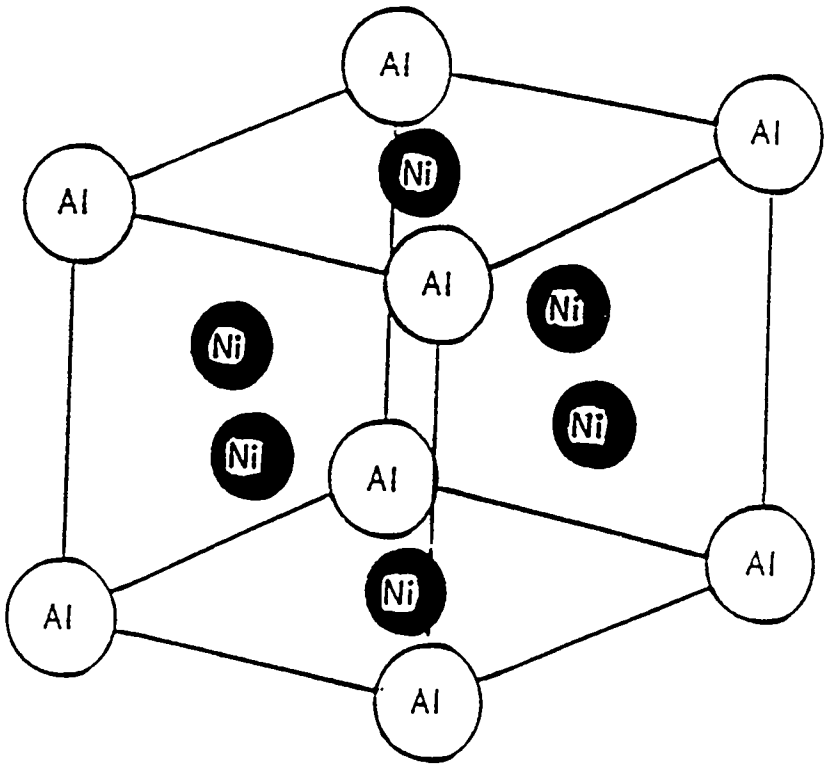

Figure 1.1 The $L1_2$ crystal structure (FCC derivative). Black circles represent Ni, White Al.

a. APB on (111)

$[\bar{1}\,0\,1] = 1/2[\bar{1}\,0\,1] + 1/2[\bar{1}\,0\,1]$

b. APB + CSF on (111)

$[\bar{1}\,0\,1] = 1/6[\bar{1}\,\bar{1}\,2] + 1/6[\bar{2}\,1\,1] + 1/6[\bar{1}\,\bar{1}\,2] + 1/6[\bar{2}\,1\,1]$

c. SISF on (111)

$[\bar{1}\,0\,1] = 1/3[\bar{2}\,1\,1] + 1/3[\bar{1}\,\bar{1}\,2]$

d. APB, CSF & SISF on (111)

$[\bar{1}\,0\,1] = 1/6[\bar{1}\,\bar{1}\,2] + 1/6[\bar{2}\,1\,1] + 1/6[\bar{1}\,2\,\bar{1}] + 1/6[1\,\bar{2}\,1] + 1/6[\bar{1}\,\bar{1}\,2] + 1/6[\bar{2}\,1\,1]$

e. SISF & SESF on (111)

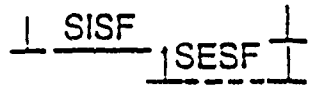

$[\bar{2}\,1\,1] = 1/3[\bar{1}\,2\,\bar{1}] + 1/3[\bar{1}\,\bar{1}\,2] + 1/3[\bar{2}\,1\,1] + 1/3[\bar{2}\,1\,1]$

Figure 2.1 Possible modes of dislocation dissociations in $L1_2$ structure. Notation described in text.

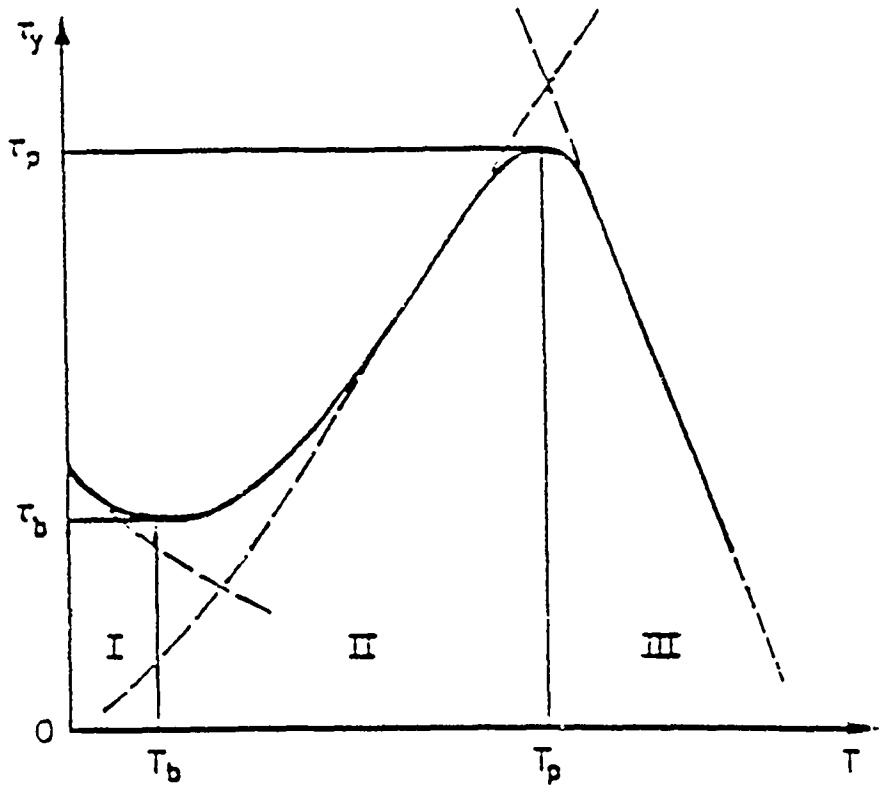

Figure 2.2 The three characteristic regions of temperature dependence of flow stress in Ni_3Al alloys.

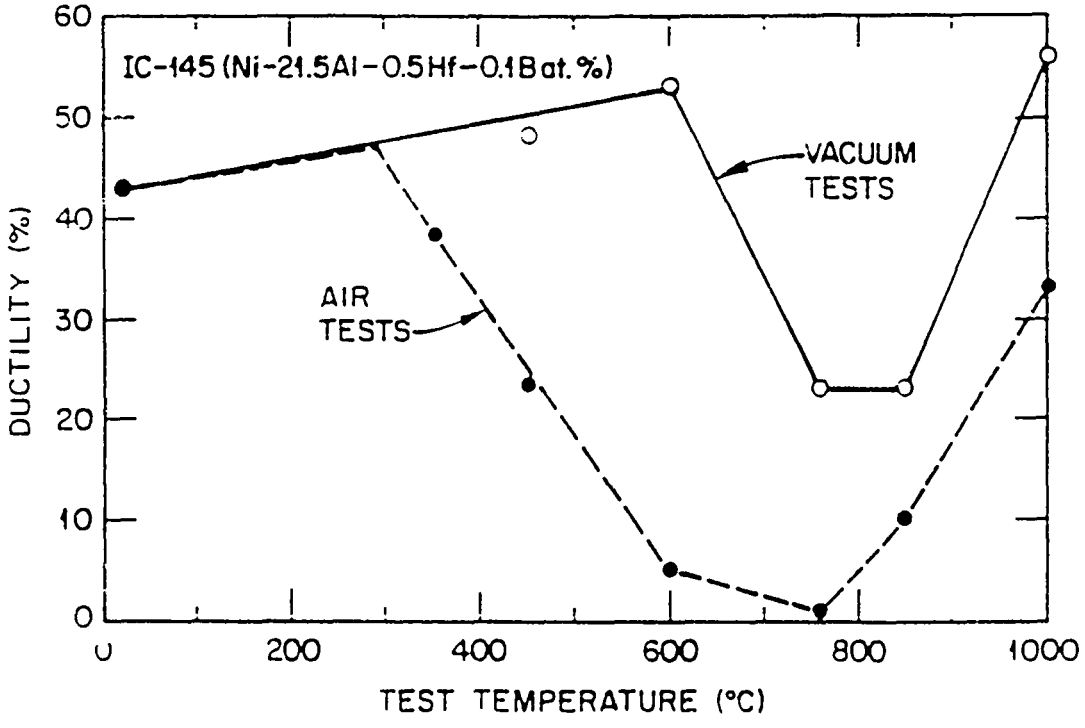

Figure 2.3 Comparison of tensile elongation of Ni-21.5 Al-0.5 Hf 0.1 B (at%) tested in vacuum and air [4].

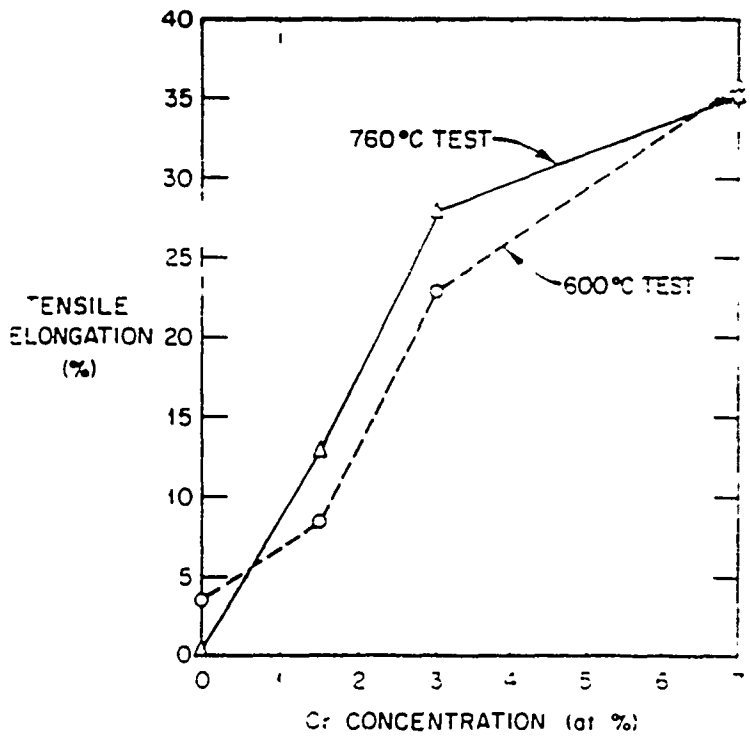

Figure 2.4 Plot of tensile elongation as a function of chromium concentration in Ni_3Al + 15.5 at.% Fe at 700° C in air [5].

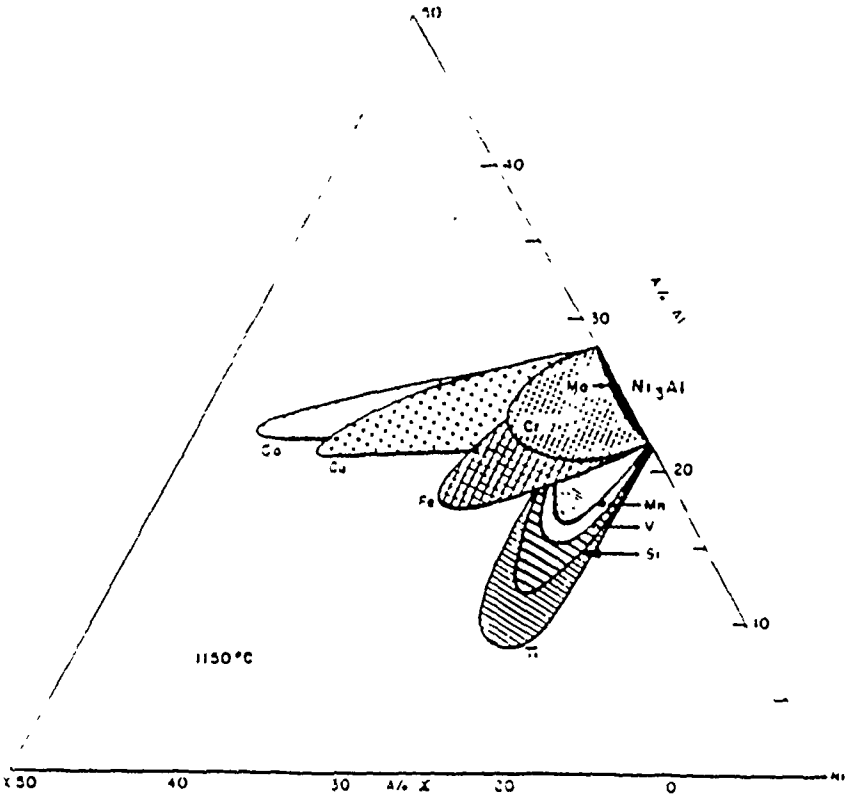

Figure 3.1 Effect of ternary element addition on phase field stability of Ni-Al-X [56]

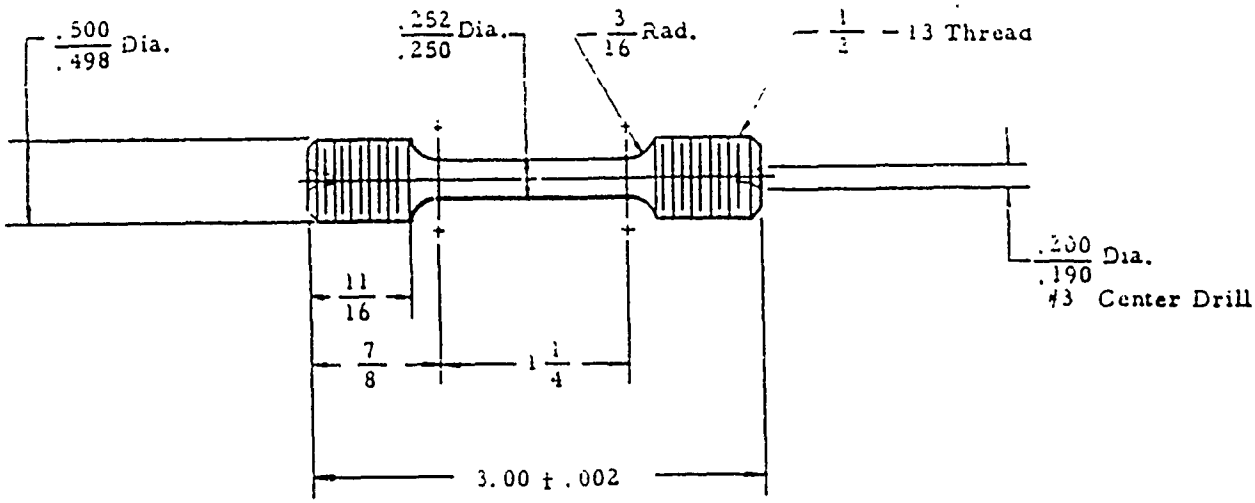

Figure 3.2 Configuration of tensile specimens utilized during the course of the research. (All dimensions in inches).

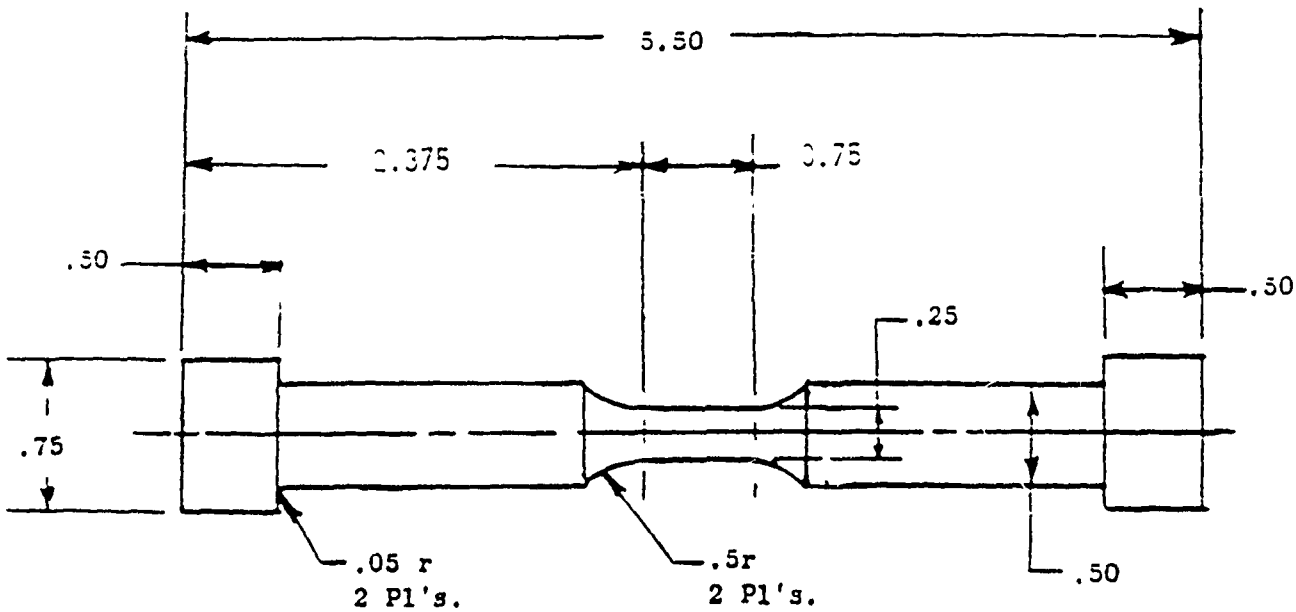

Figure 3.3 Configuration of the low cycle fatigue (LCF) specimens utilized during the course of the research. (all dimensions in inches).

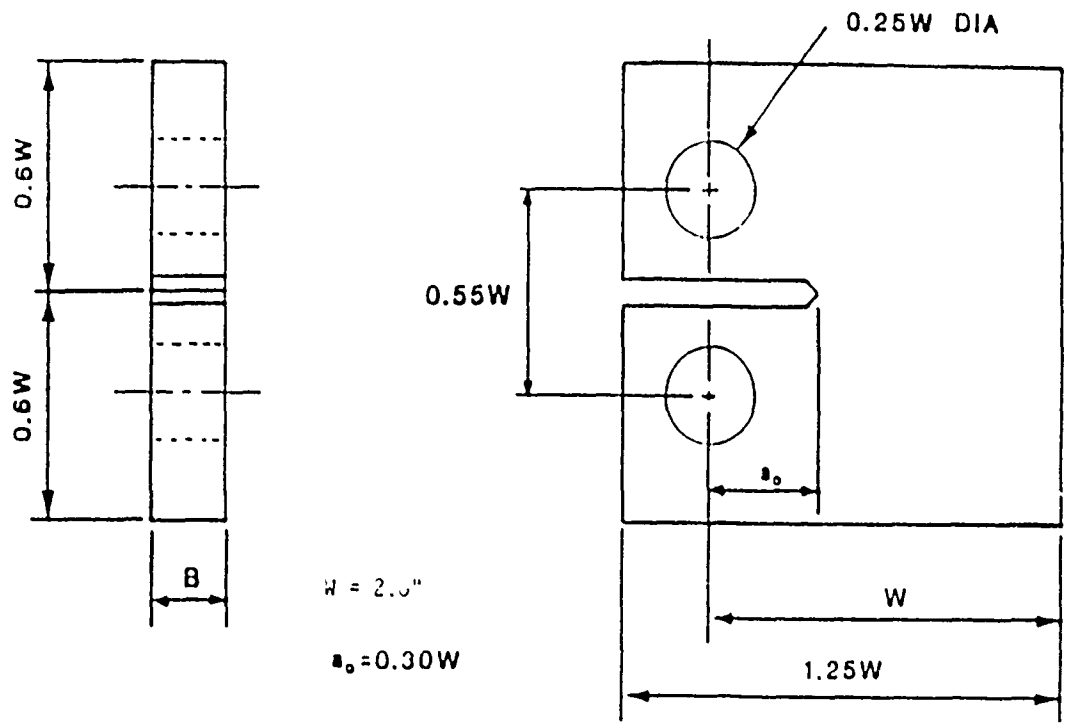

Figure 3.4 Configuration of the compact test (CT) fatigue crack propagation (FCP) specimens utilized during the course of the research.

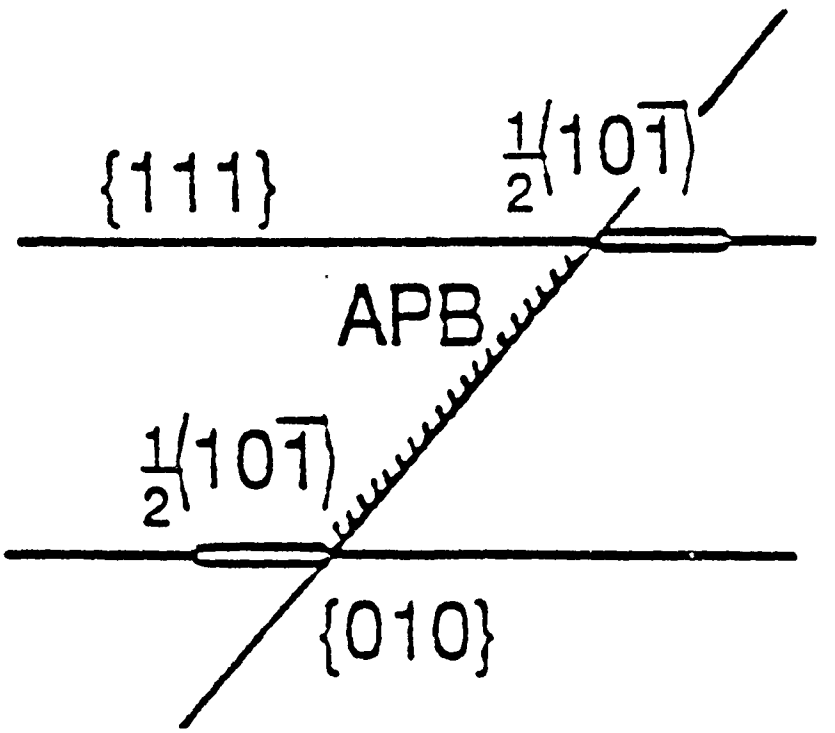

Figure 4.1 The Kear-Wilsdorf cross-slip configuration in Ni_3Al.

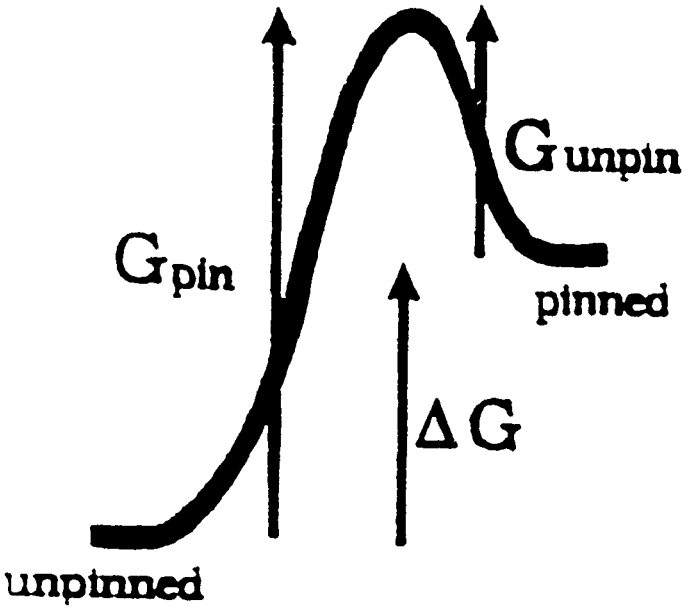

Figure 4.2 Schematic representation of the energy barriers to forward and reverse cross-slip.

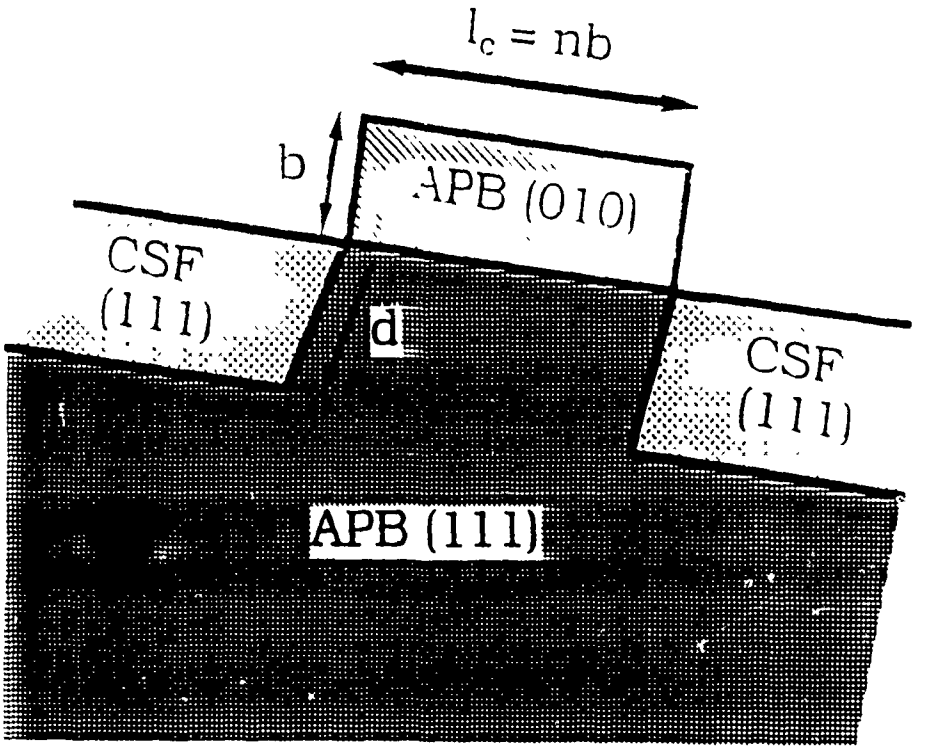

Figure 4.3 Schematic representation of the highest energy configuration of a cross-slipped segment.

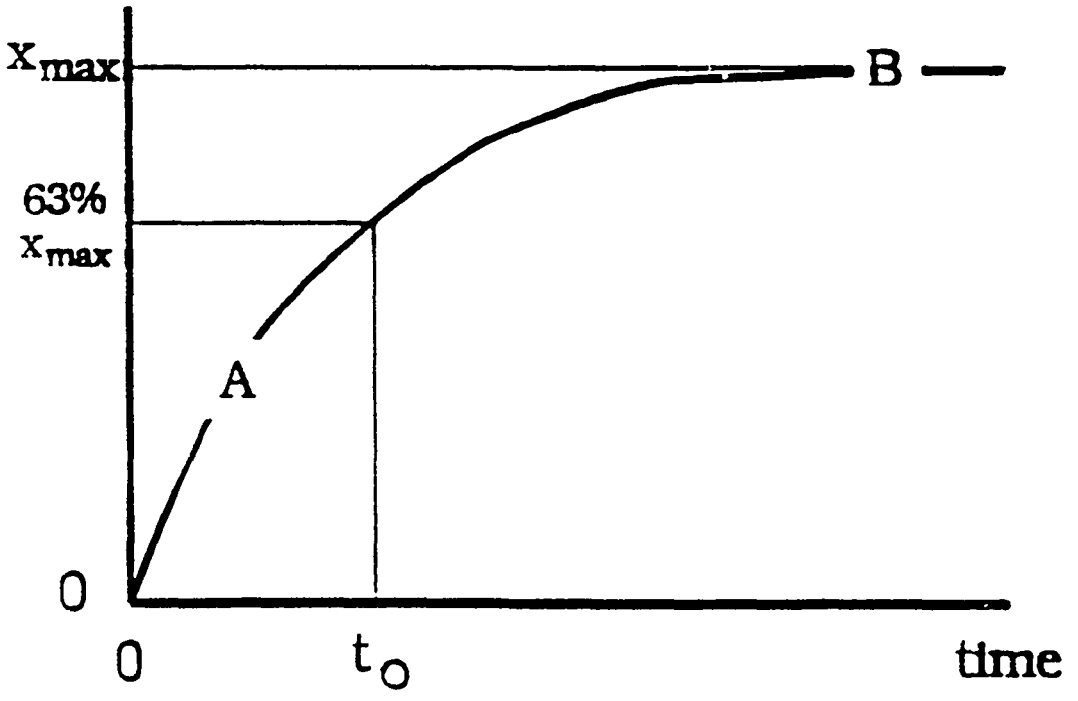

Figure 4.4 Variation in dislocation cross-slip segment accumulation with time.

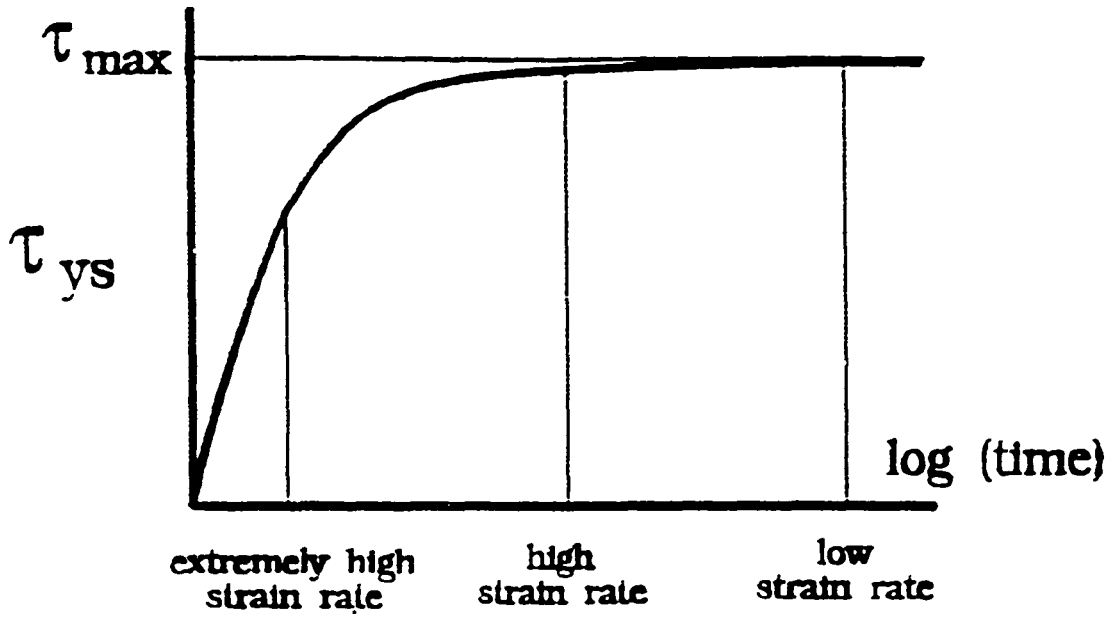

Figure 4.5 Variation in the flow stress (intrinsic resistance) as a function of time.

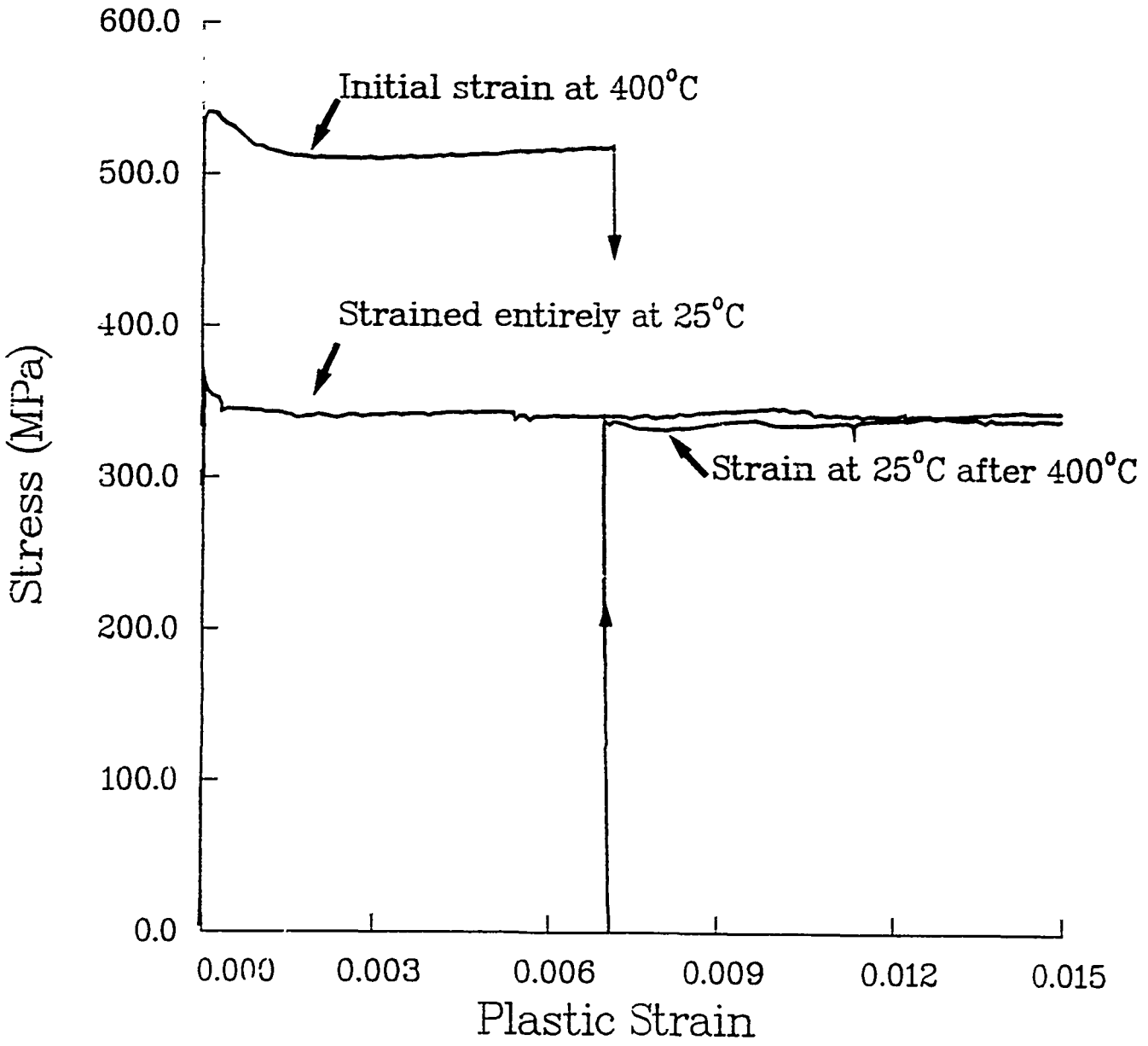

Figure 4.6 Results from Cottrell-Stokes experiment. Specimen was initially strained 1% at 400° C, then restrained at 25° C an additional 1% demonstrating complete thermal reversibility.

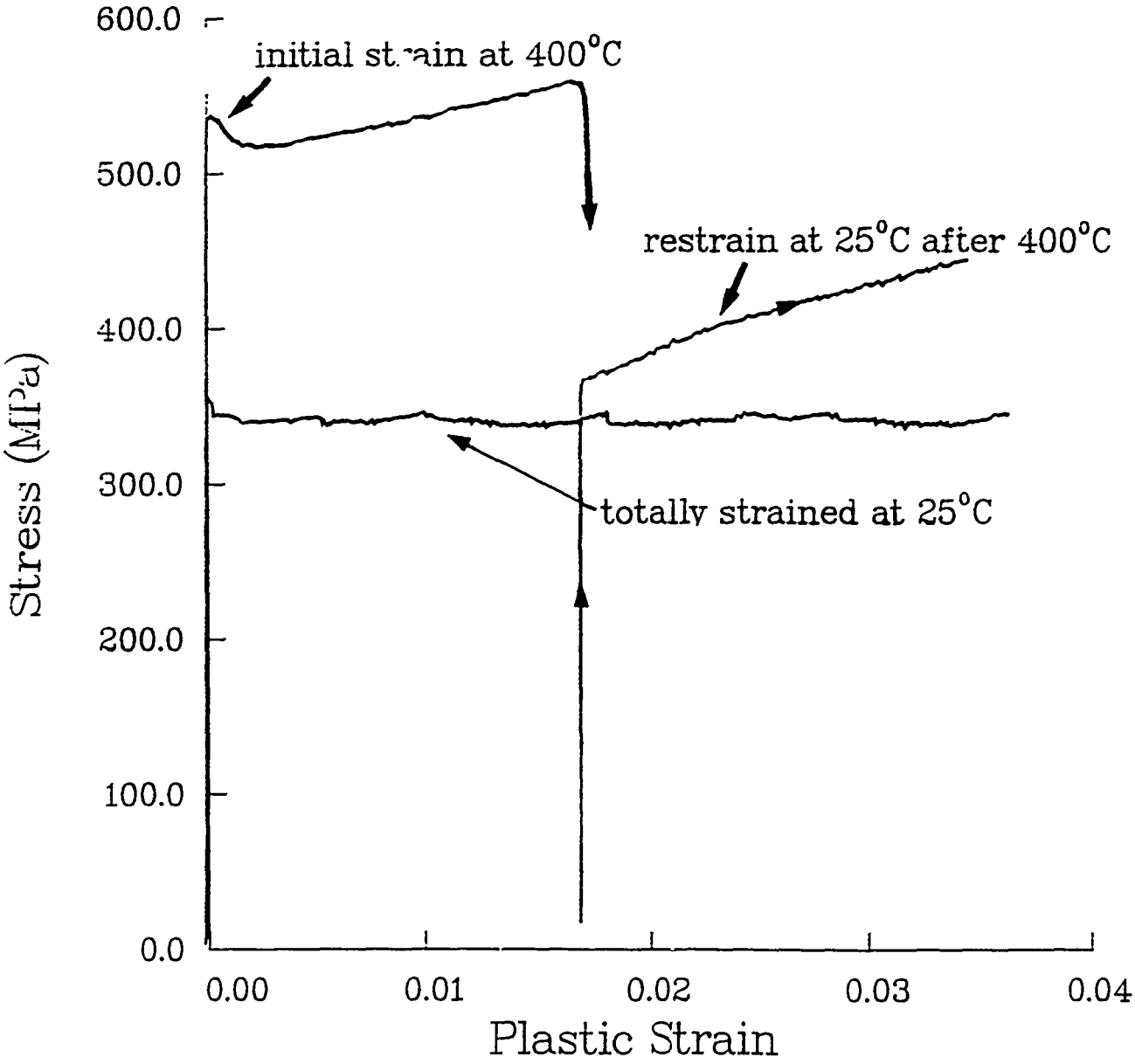

Figure 4.7 Results from Cottrell-Stokes experiment. Specimen was initially strained 2% at 400° C, then restrained at 25° C 2%. Results indicate partial irreversibility consistent with the observed increase in flow stress at 400°C.

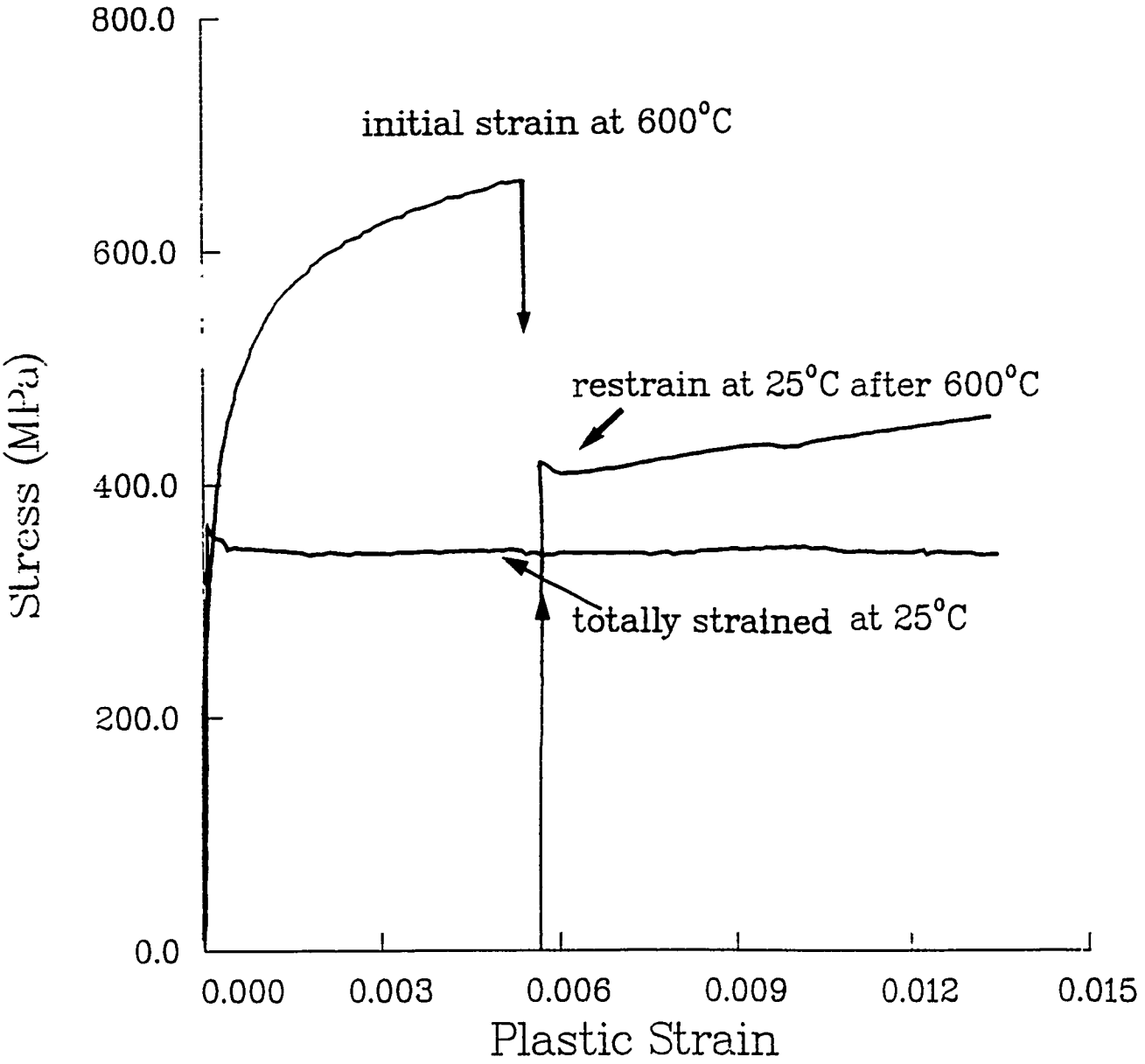

Figure 4.8 Results from Cottrell-Stokes experiment. Specimen was initially strained 1% at 600° C, then restrained 1% at 25°C. Irreversibility is related to the presence of dislocations on cube planes which gives rise to the observed irreversibility.

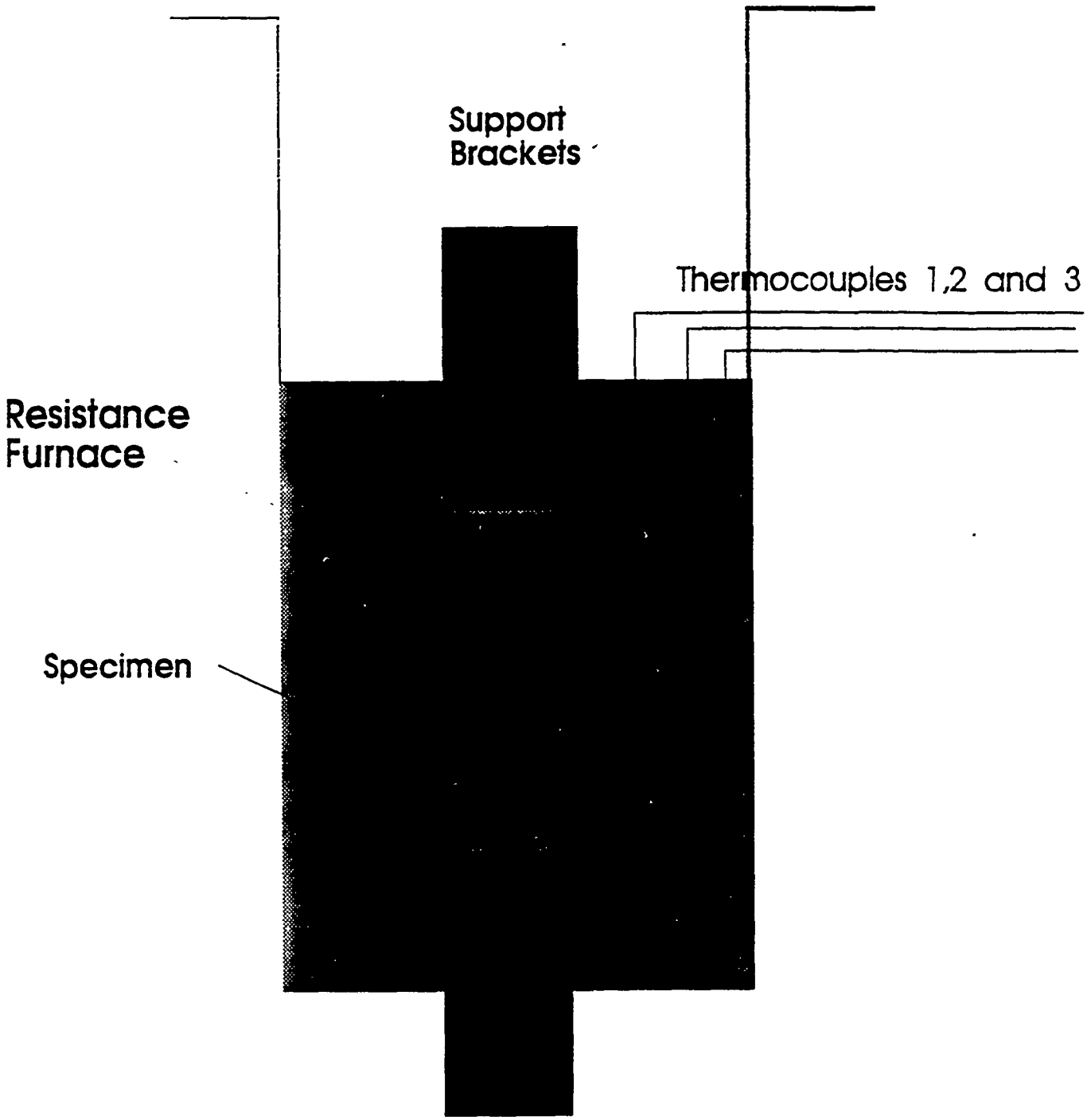

Figure 5.1 Configuration of furnace and specimen during elevated temperature tensile testing in a vacuum environment.

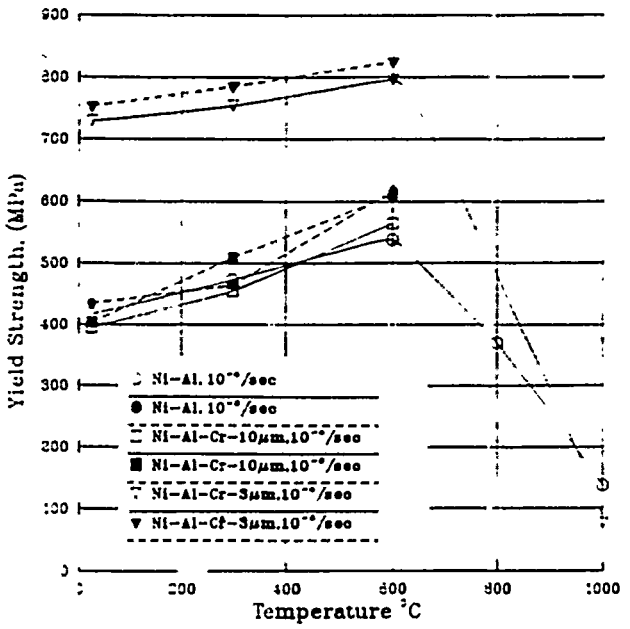

A.

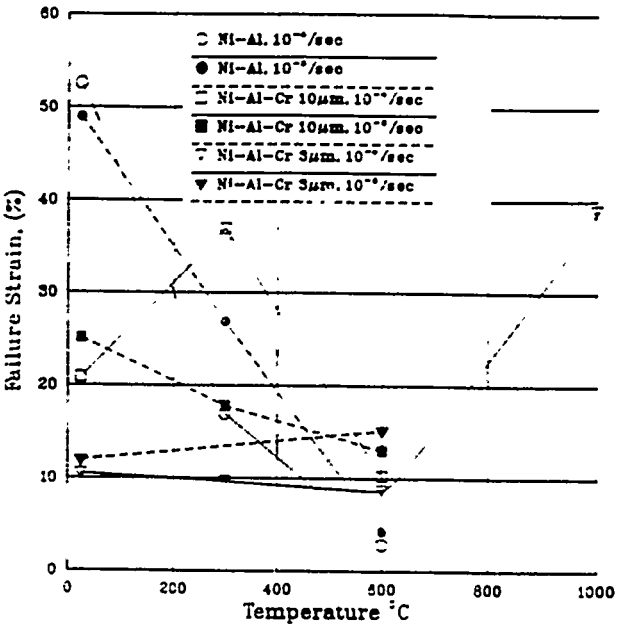

B.

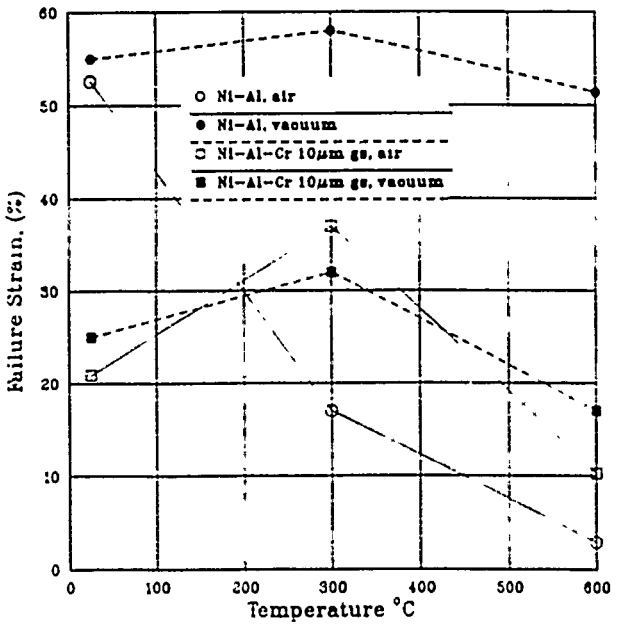

C.

Figure 5.2 Temperature dependence of monotonic properties of the experimental alloys. (a) Yield Strength (b) Elongation to failure in air (c) Elongation to failure in vacuum and air.

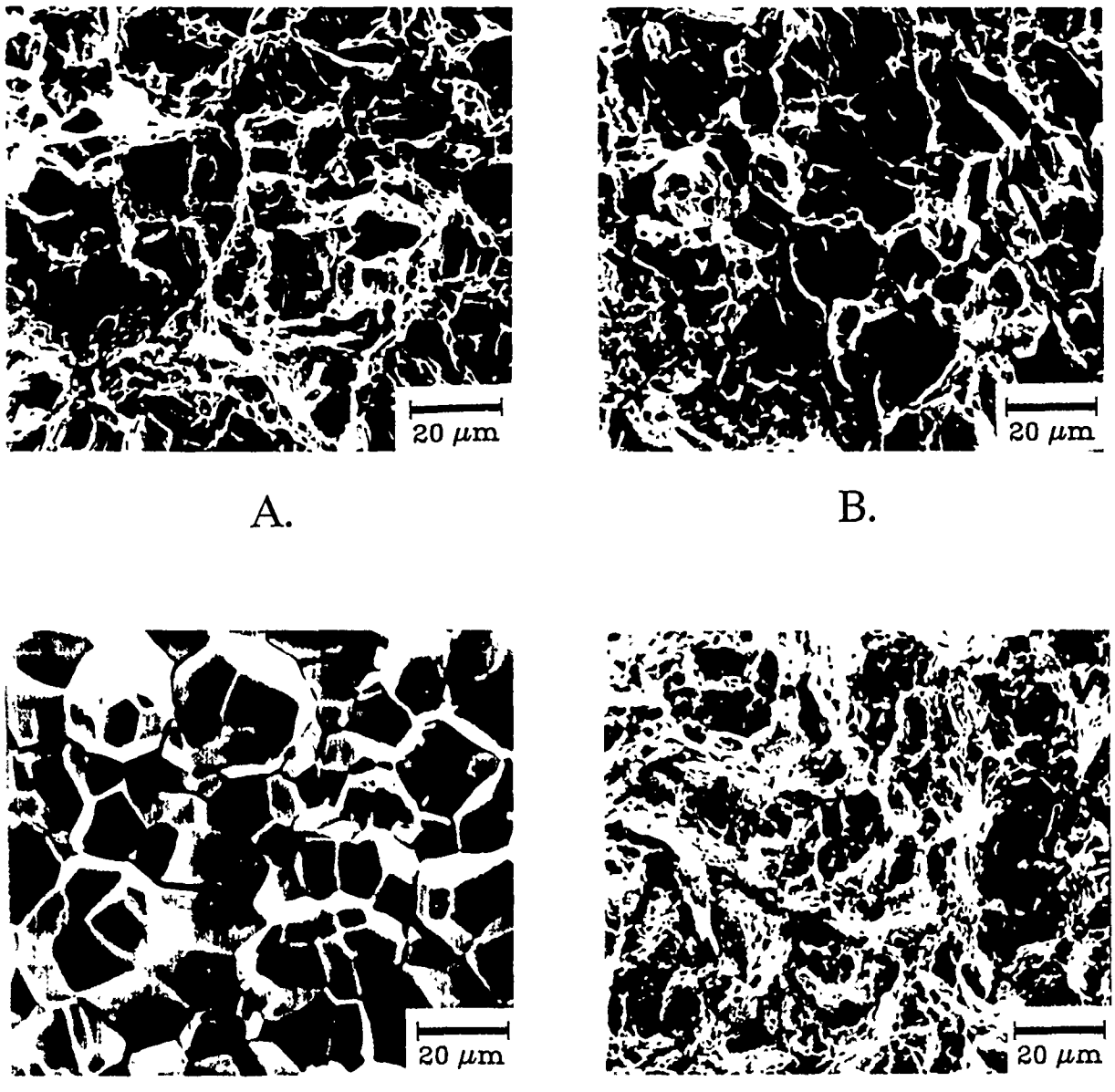

Figure 5.3 Changes in tensile fracture surface morphology of the binary alloy with temperature and environment. (a) 25°C, air (b) 300°C, air (c) 600°C, air (d) 600°C, vacuum.

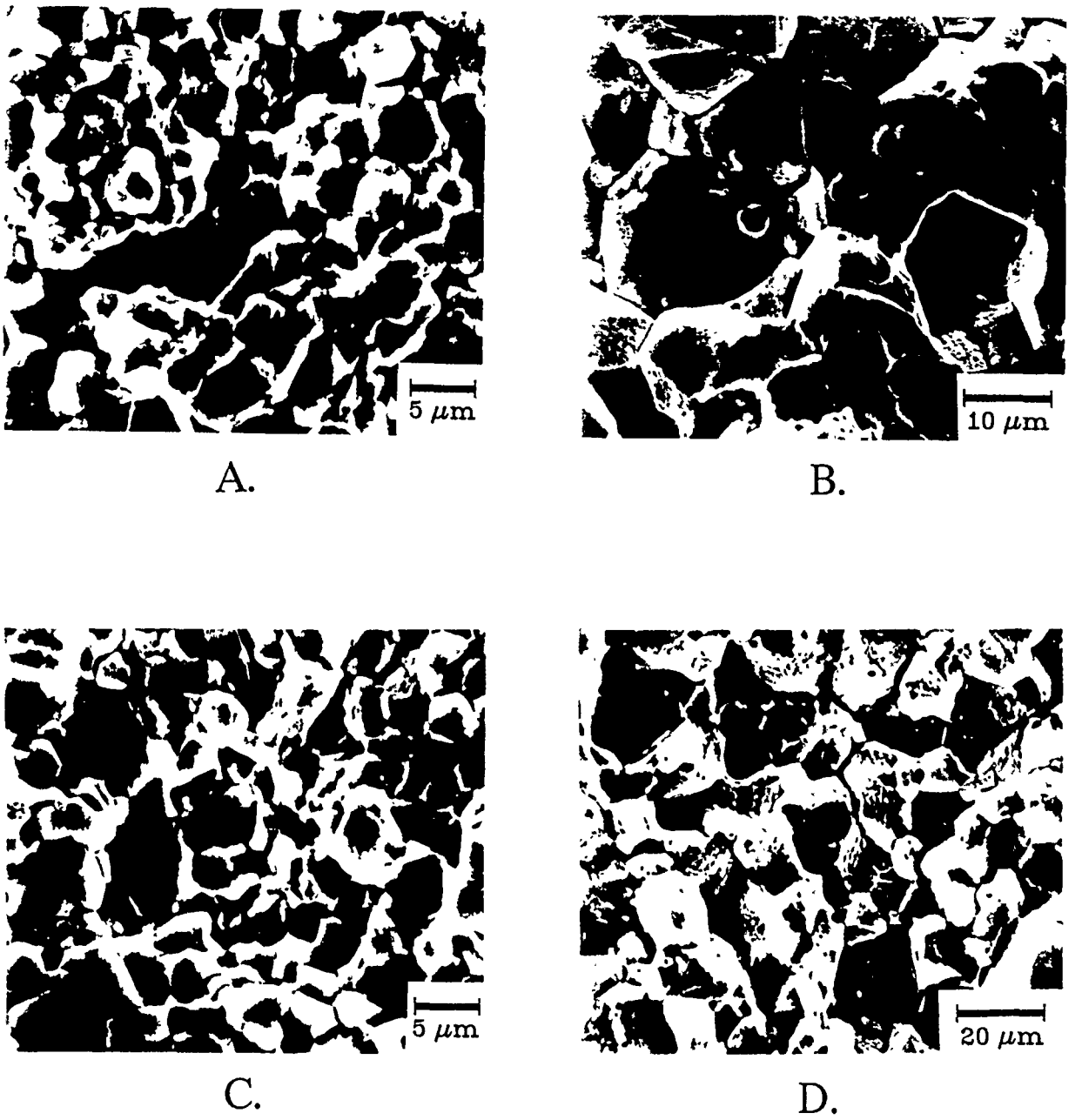

Figure 5.4 Fracture surface morphology of ternary alloys as a function of temperature and grain size. (a) 25°C, 3.5μm gs (b) 25°C, 10.1μm gs (c) 600°C, 3.5μm gs (d) 600°C, 10.1μm gs.

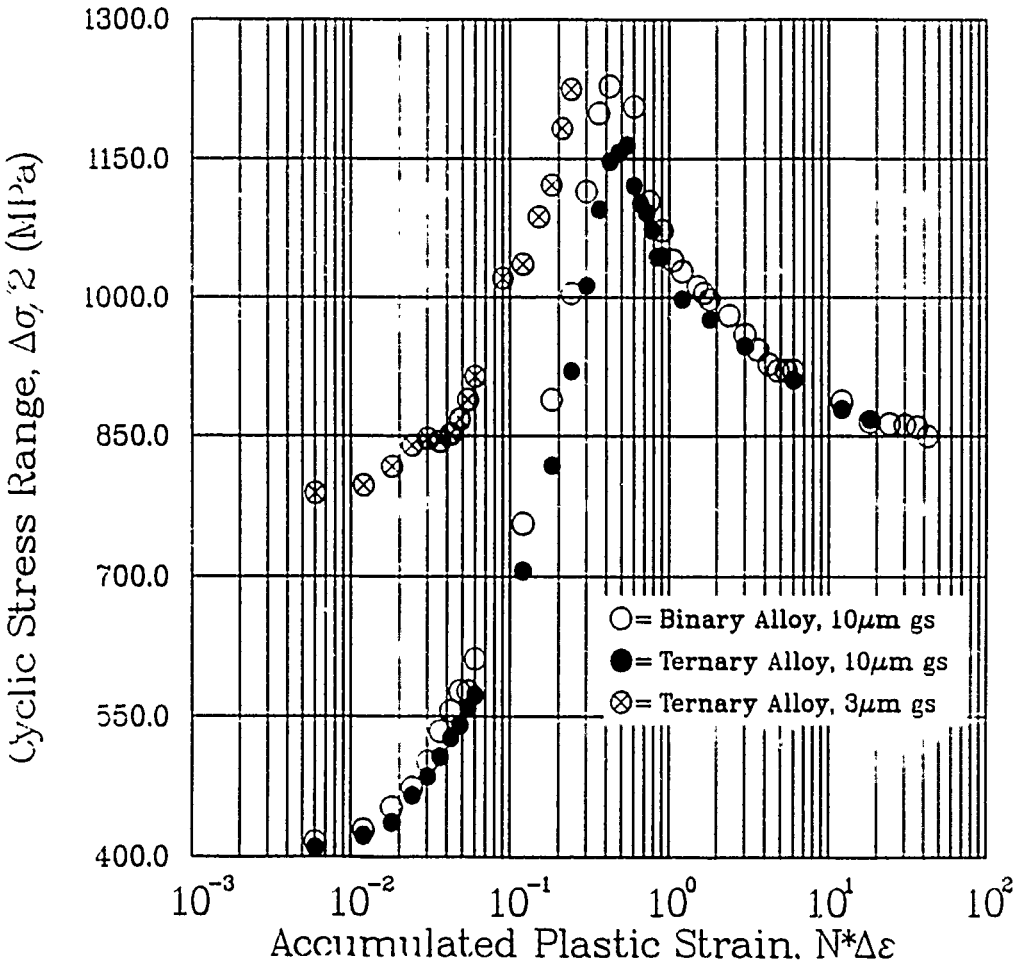

Figure 6.1 Cyclic hardening and softening characteristics at 25°C of experimental Ni_3Al alloys. The mean cyclic stress range is plotted verse the accumulated plastic strain to fracture.

1 Reversal

A.

30 Reversals

B.

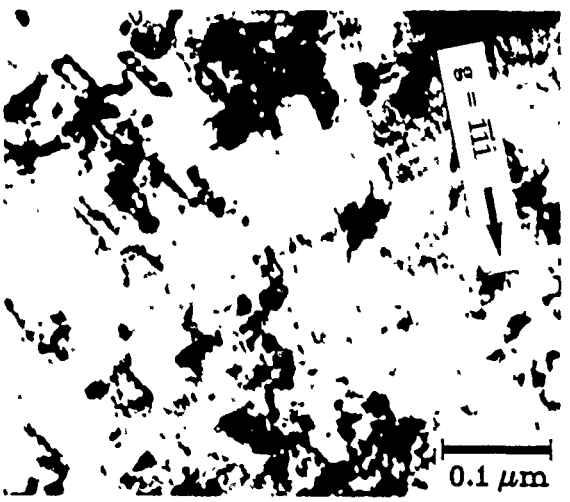

100 Reversals

C.

Figure 6.2 Characteristics of deformation in Ni_3Al during cyclic hardening at ambient temperature. TEM photomicrographs all utilize **g** = <111>, for maximum visibility of dislocations with **b** = <110>. Note the increasing density of faulted SISF loops (a) 1 reversal, $\Delta\epsilon_p$ = 0.006 (b) 10 reversals, $\Delta\epsilon_p$ = 0.006 (c) 100 reversals, $\Delta\epsilon_p$ = 0.006.

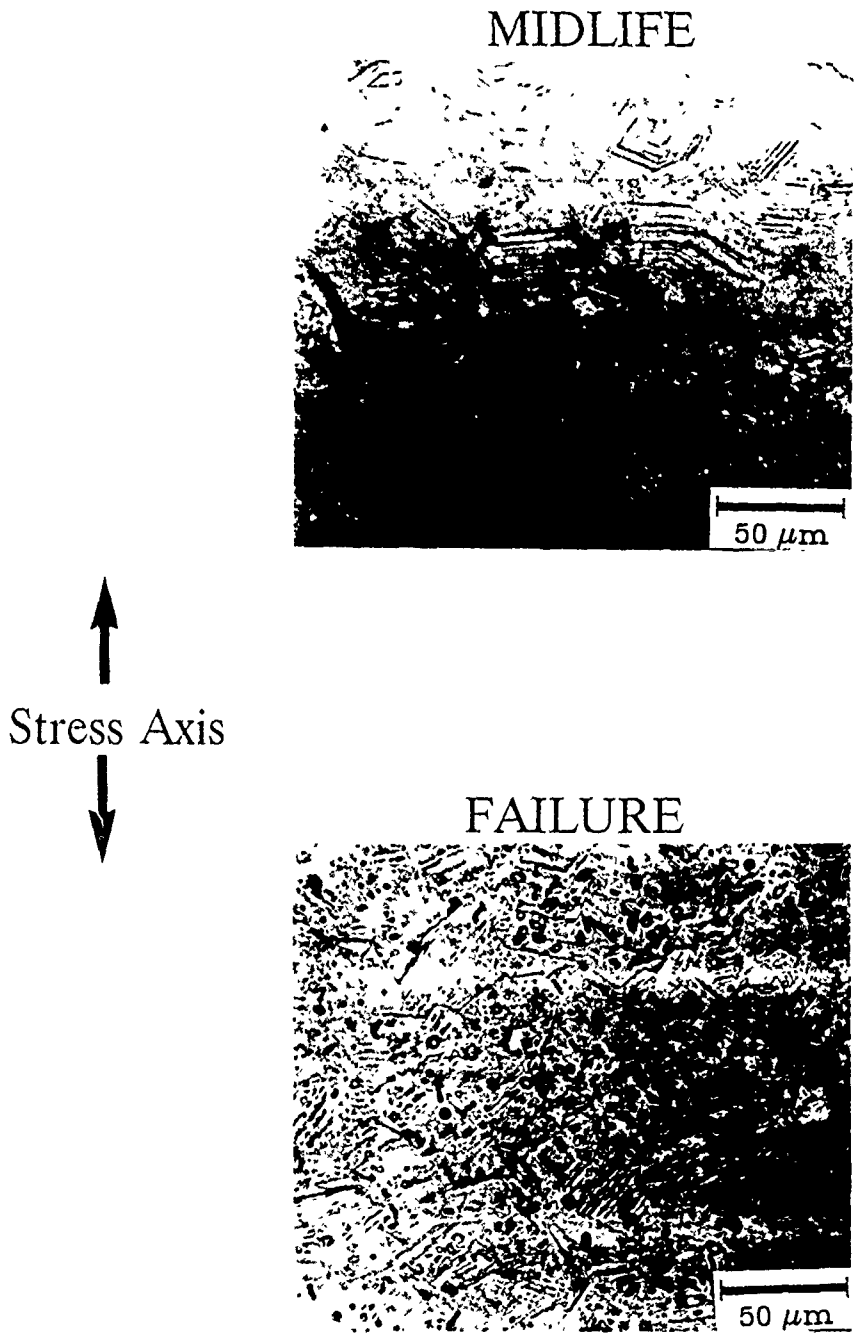

Figure 6.3 Characteristics of deformation during softening in Ni_3Al at ambient temperature. Replication of specimen surfaces at midlife and failure indicating planar slip traces which result in crack nucleation.

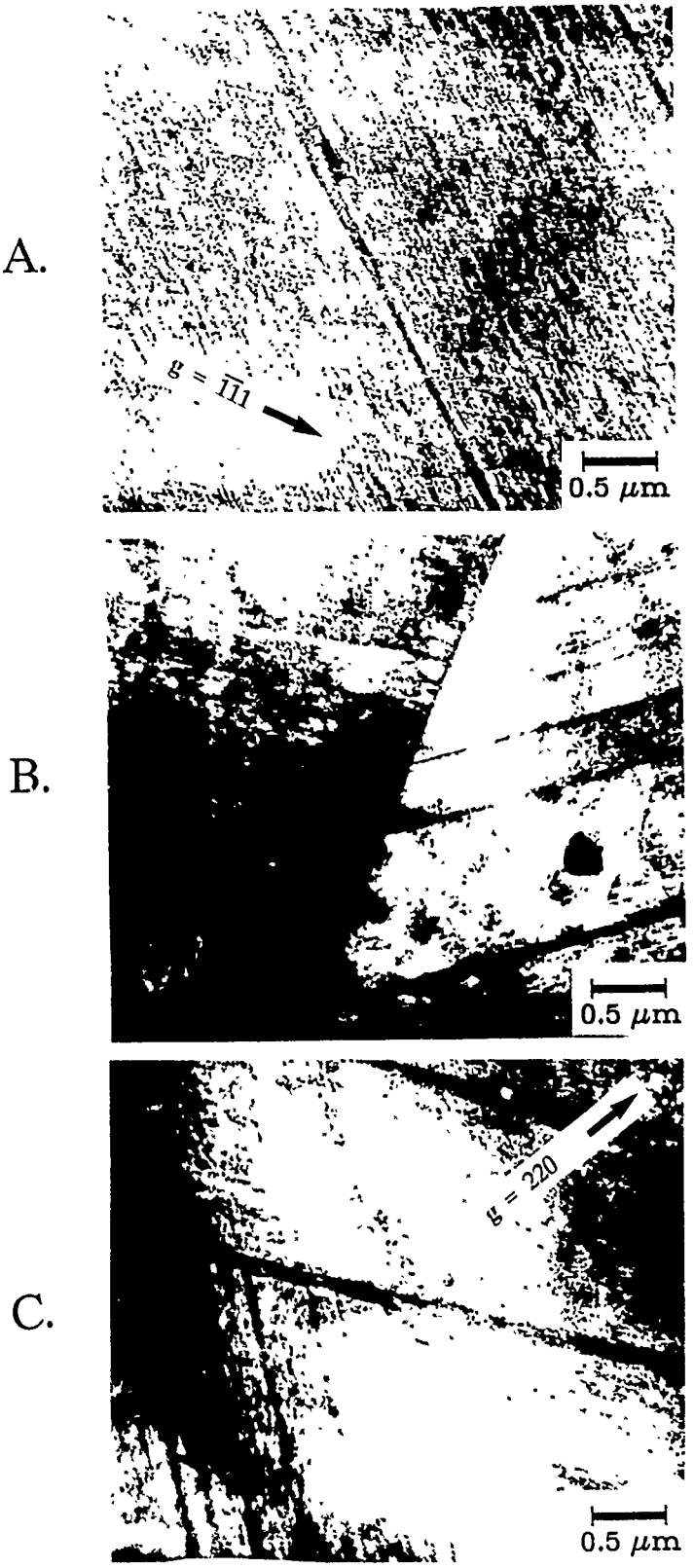

Figure 6.4 Characteristics of deformation during softening in Ni_3Al at ambient temperature. TEM investigation of slip bands reveal. (a) slip bands passing through homogeneous distribution of SISF loops (b) Slip band intersection at grain boundaries (c) Slip band intersection within grains.

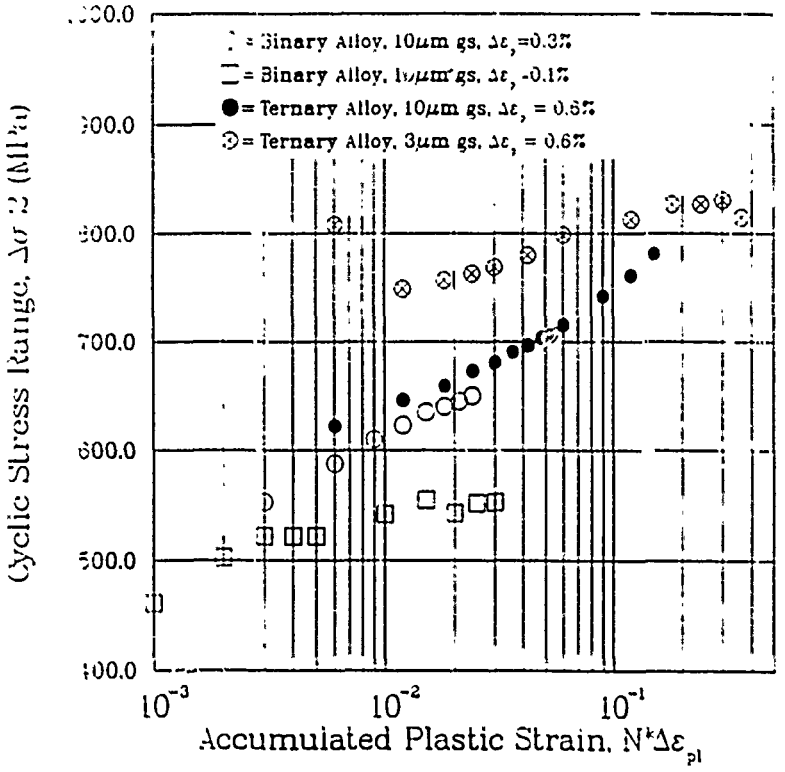

A.

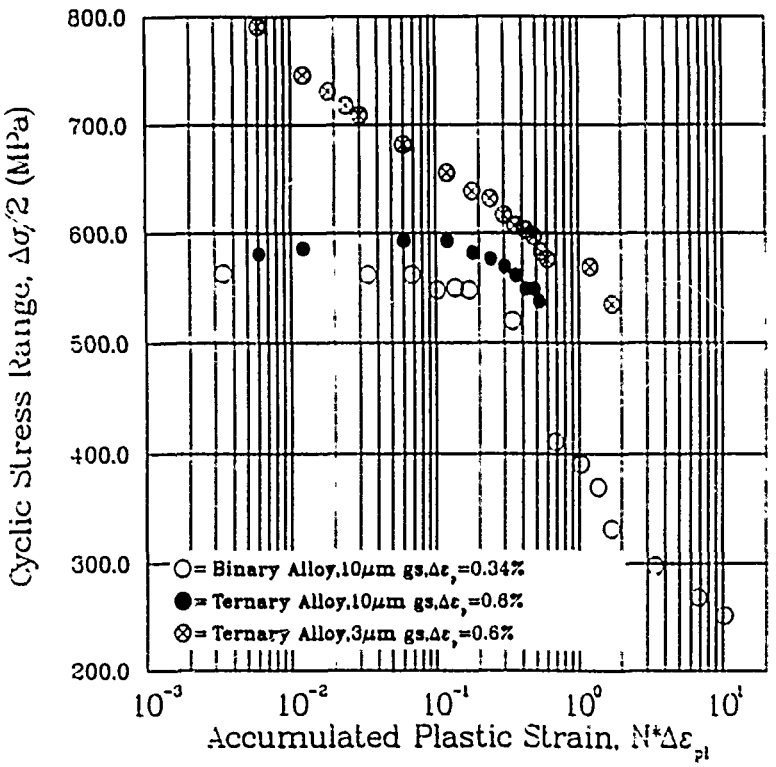

B.

Figure 6.5 Cyclic hardening and softening characteristics at 600° C of experimental Ni_3Al alloys when tested at strain rates of (a) 10^{-2}/sec and (b) 10^{-4}/sec.

A.

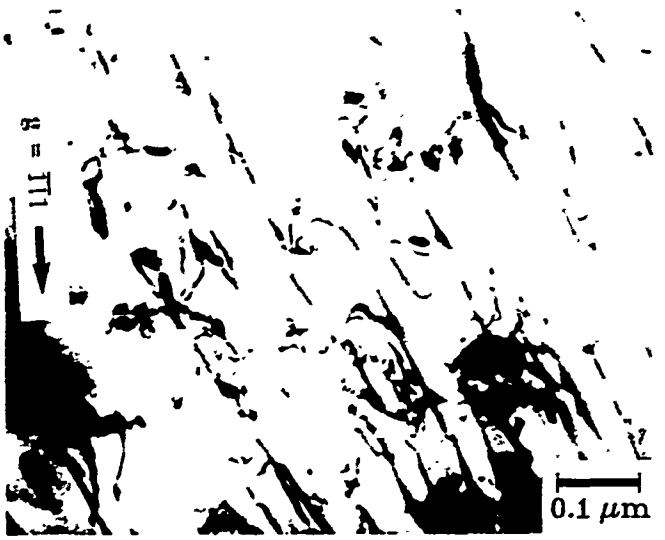

B.

Figure 6.6 Characteristics of deformation during deformation of Ni_3Al at 600° C at strain rates of (a) 10^{-2}/sec and (b) 10^{-4}/sec.

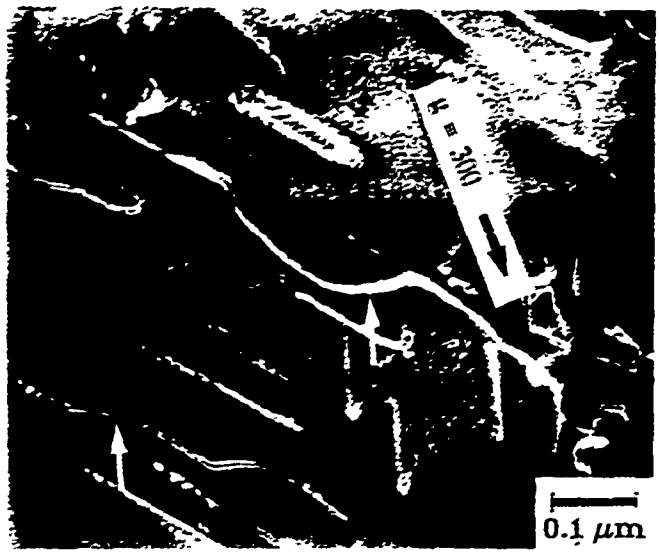

A.

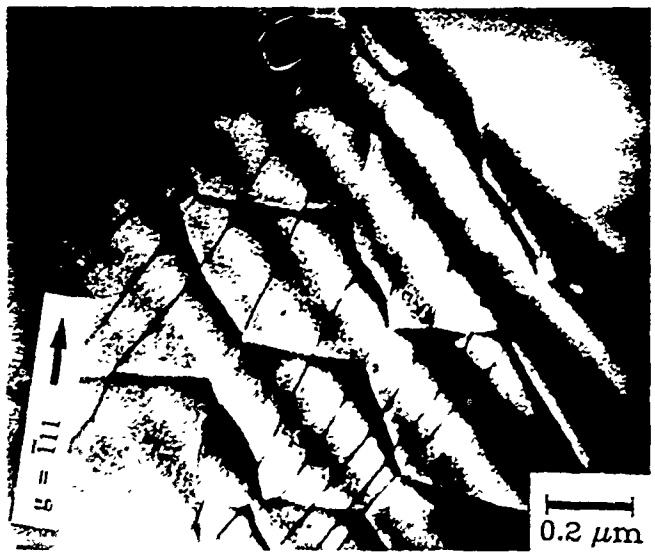

B.

Figure 6.7 Indications of thermally activated dislocation motion during deformation of Ni_3Al at 600° C at a rate of 10^{-4}/sec. (a) weak beam g = [100], bowing of screw dislocations onto cube planes arrows [B = 010]. Grain boundary dislocation networks.

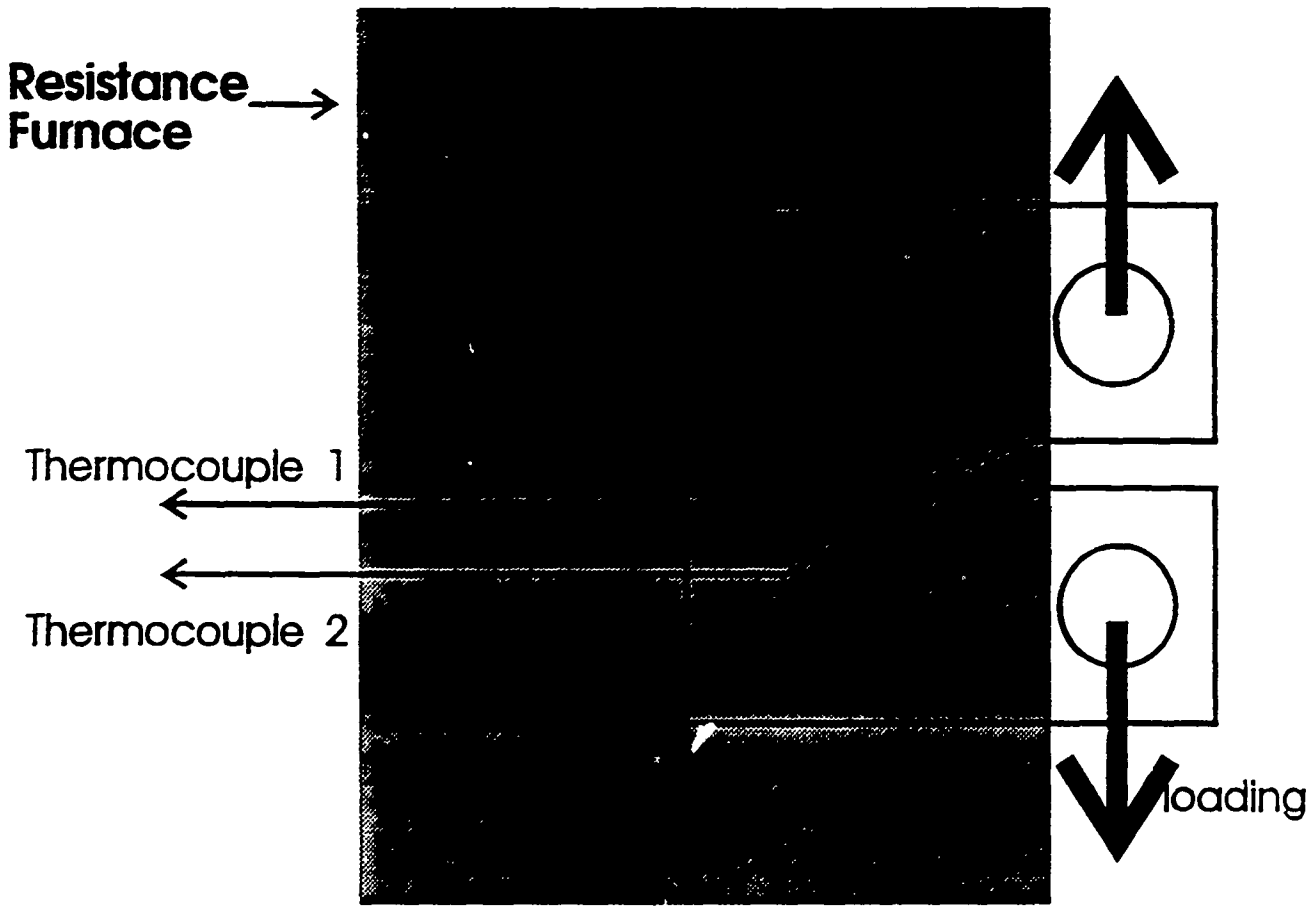

Figure 7.1 Schematic configuration of furnace, specimen and thermocouples during fatigue crack propagation testing in vacuum environments

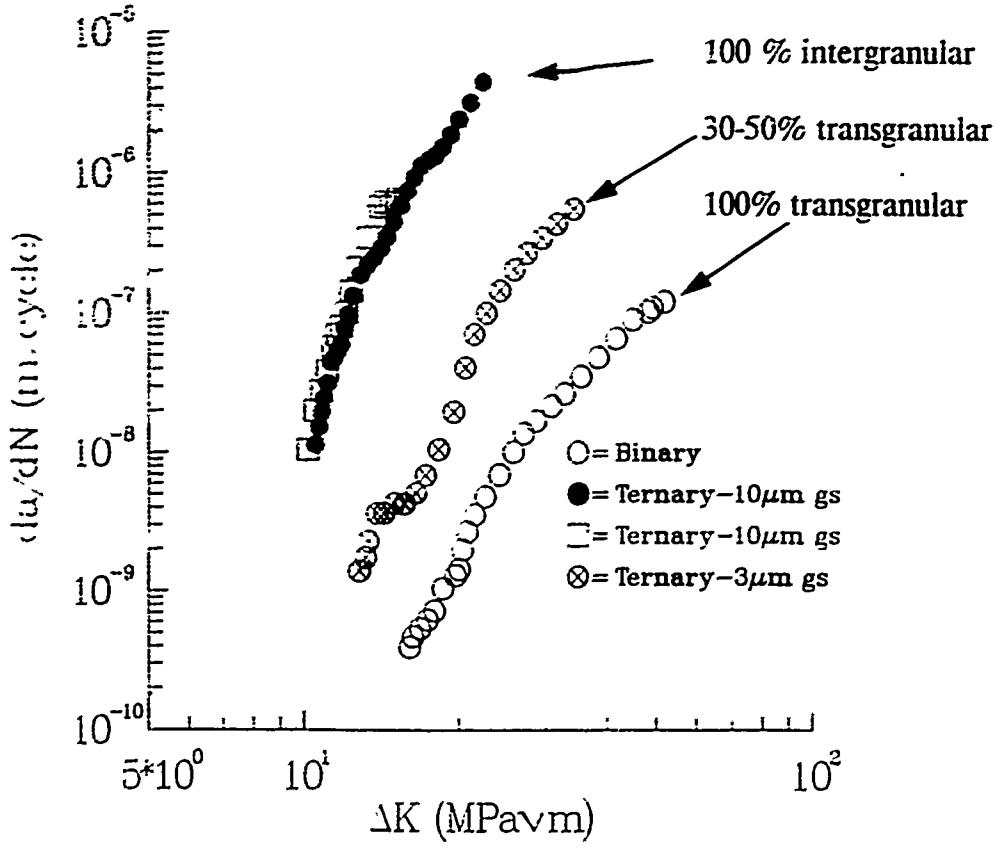

Figure 7.2 Fatigue crack growth rates of the binary and ternary alloy, 25°C, air, R=0.1, ν = 10 Hz.

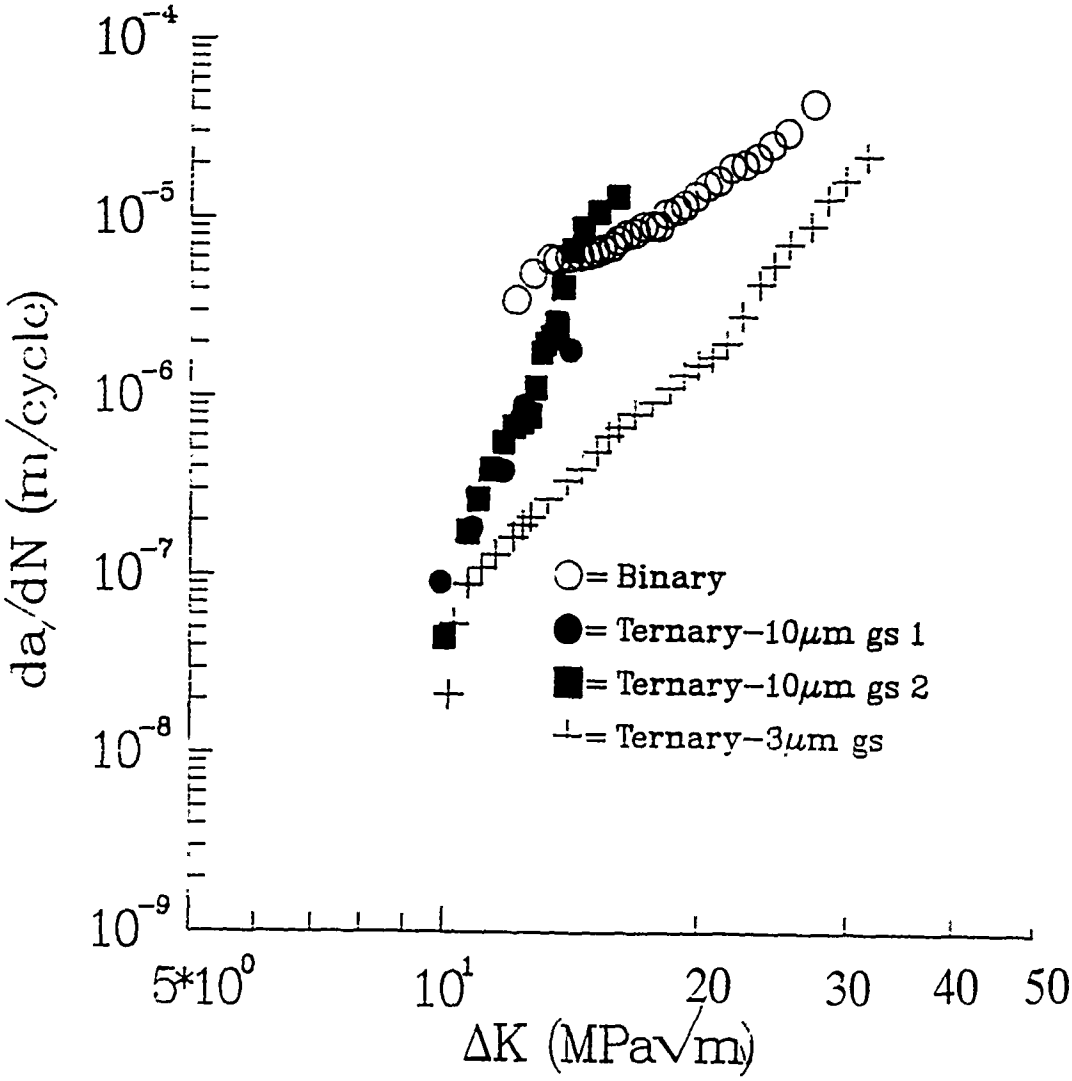

Figure 7.5 Comparison of fatigue crack growth rates at 600° C for binary and ternary alloy.

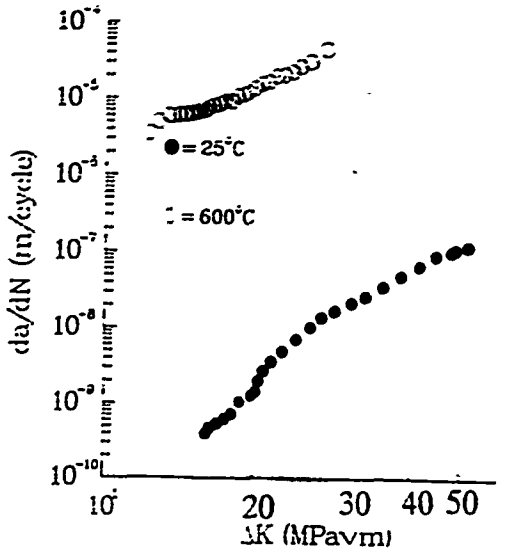

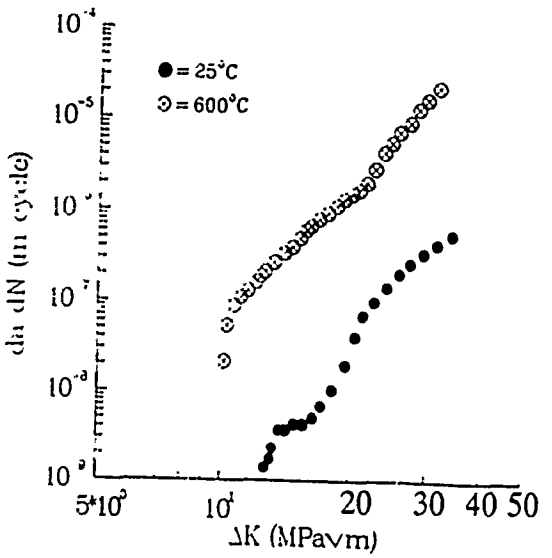

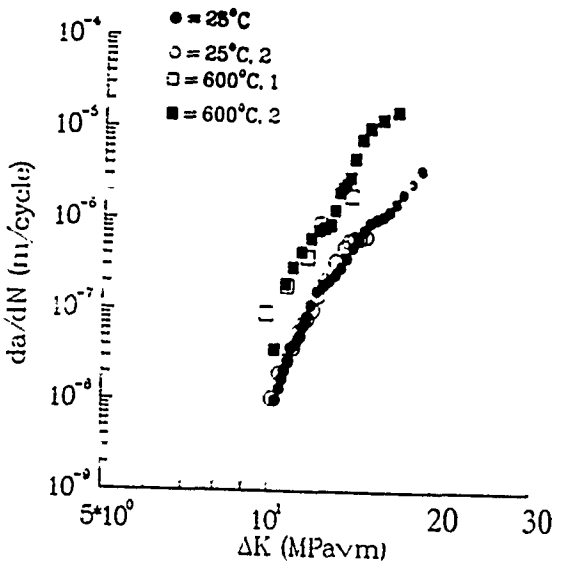

Figure 7.4 Temperature dependence of fatigue crack growth resistance in experimental binary and ternary alloys. (a) binary alloy Ni-Al, (b) ternary alloy Ni-Al-Cr, 3.5μm gs, (c) ternary alloy Ni-Al-Cr 10.1μm

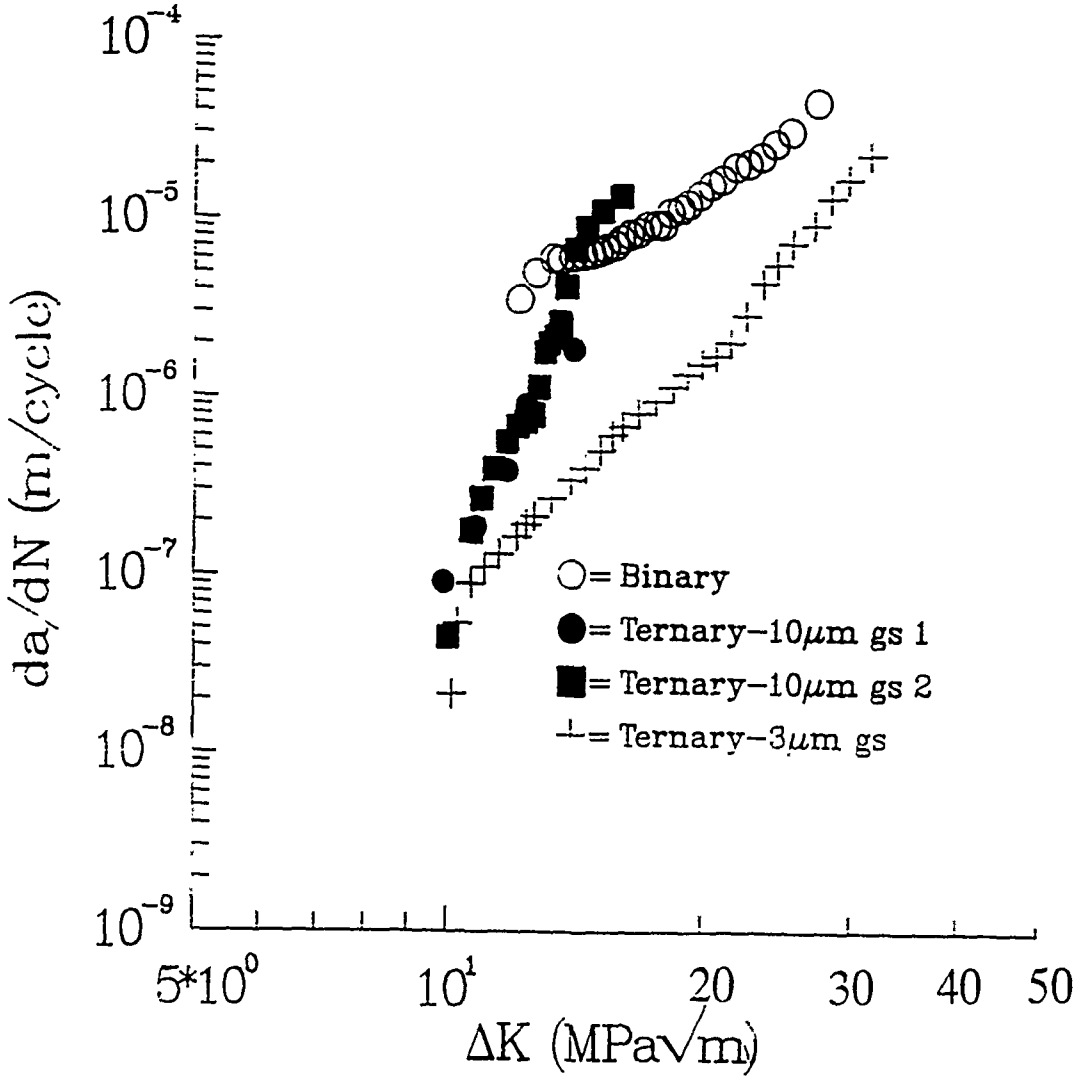

Figure 7.5 Comparison of fatigue crack growth rates at 600° C for binary and ternary alloy.

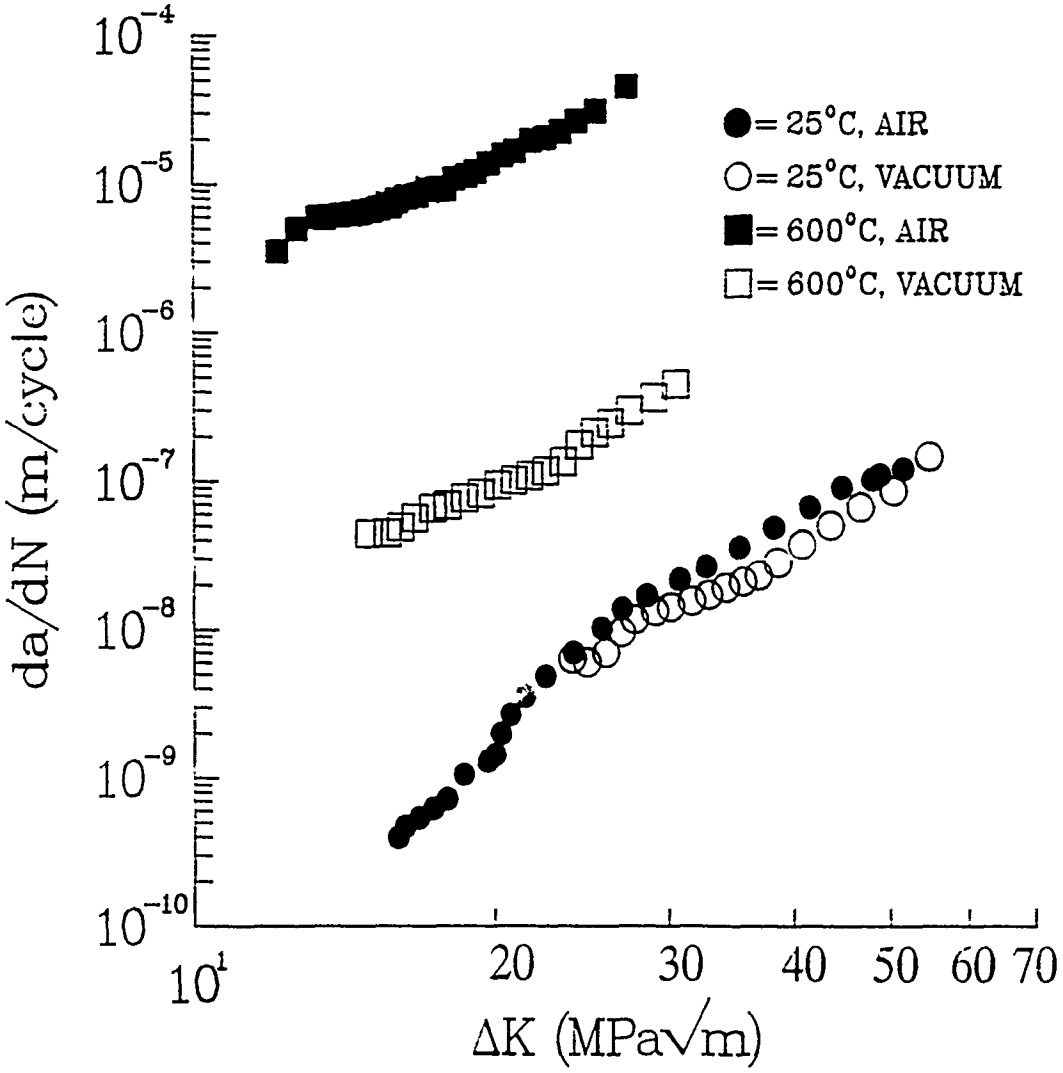

Figure 7.6 Dependence of fatigue crack growth rate on test environment and temperature for the binary alloy.

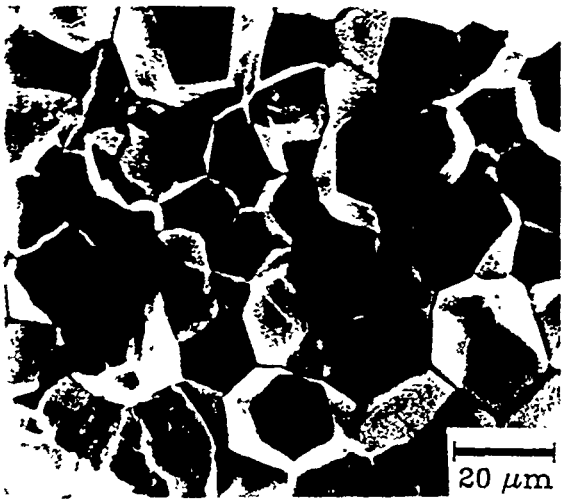

A.

← Crack Growth

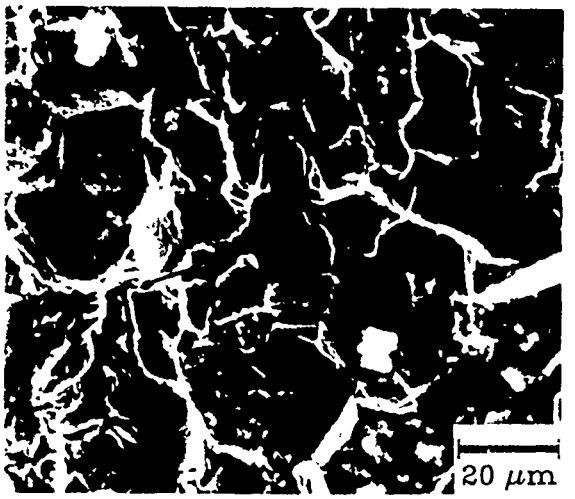

B.

Figure 7.7 Fracture surface morphology of fatigue crack growth of binary alloy at 600° C in (a) air and (b) vacuum.

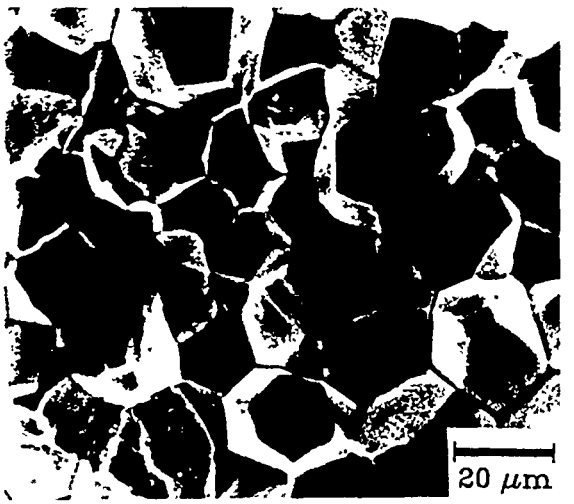

A.

← Crack Growth

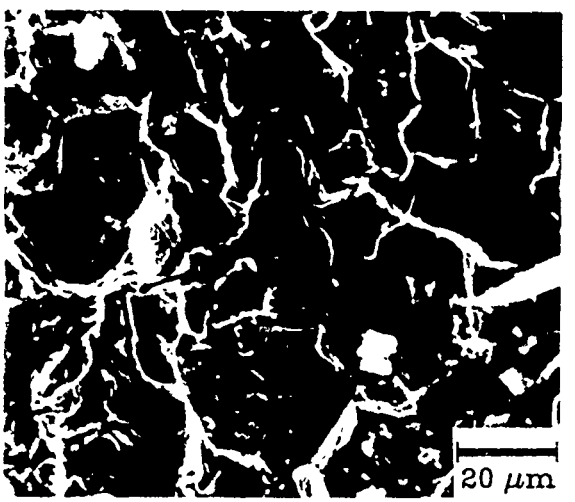

B.

Fig' re 7.7 Fracture surface morphology of fatigue crack growth of binary alloy at 600° C in (a) air and (b) vacuum.